Geometric social force interaction models for autonomous driving with mobile robots

van Kampen, R.J.R.

Award date:
2018

Geometric social force interaction models for autonomous driving with mobile robots

R.J.R. van Kampen

DC 2018.051

Master's thesis

Coach:	dr.ir. E. Steur[1,2]	Committee:	prof.dr. H. Nijmeijer[1]
			dr.ir. E. Steur[1,2]
Supervisor:	prof.dr. H. Nijmeijer[1]		dr.ir. R. Toth[3]

[1] Eindhoven University of Technology
Department of Mechanical Engineering
Section Dynamics and Control

[2] Delft University of Technology
Faculty of Mechanical, Maritime and Materials Engineering
Delft Center for Systems and Control
Section Hybrid, Adaptive & Nonlinear

[3] Eindhoven University of Technology
Department of Electrical Engineering
Section Control Systems

Eindhoven, August, 2018

Abstract

Traffic jams are an increasing problem, which can be tackled via one solution: automation. Current automation solutions are often based on stepwise protocols and require communication, therefore being only valid for very specific situations with the strict requirement of functioning communication. The goal of this thesis is to create a control strategy for autonomous (highway) driving based on interactions rules, where the desired (collective) behavior emerges from these (local) interaction rules. The desired interaction rules can be found in nature, where many examples of collective behavior exist, who do not require communication. For example, pedestrians can walk through a bottleneck scenarios without colliding and using communication. Therefore, the used framework is the social force model, used for modeling these crowd dynamics. However, nature also shows the importance of taking the dynamics into account. Therefore, the nonholonomic constraint (the no lateral slip condition) which is often a property of vehicles, is included in the model. The interactions of the social force model and inclusion of the constraint will be tested on a road narrowing scenario.

In the social force model each agent has a circular comfort zone. If two comfort zones overlap, the agent experience a force based on the overlap. Due to the overlap, both agents will react accordingly to the defined interaction rules. An agent who's comfort zone is violated at the back will have the tendency to drive faster while the tailgating agent will slow down. In the chosen road narrowing scenario this results in agents "pushing" other agents through the road narrowing. Therefore, the average flow time of agents traveling through the road narrowing is close to the nominal flow time. Agents at the front will drive faster than their desired speed, while agents at the back drive slower. Hence, the agents share discomfort and collaborate to achieve a better flow through the road narrowing without using communication.

To improve the throughput even further the comfort zone radius is linearly depending on the speed (constant time spacing policy). By applying the spacing policy, an agent only uses the required amount of road without reducing safety. However, introducing the spacing policy also requires taking care of the road's geometry since it is undesirable to have a comfort zone much smaller or wider than the lane width. The inclusion of geometry causes different problems. Using the circular comfort zones, the measure of violation is isotropic (direction independent). The inclusion of geometry requires a direction dependent measure of comfort zone violation. Geometry is included by applying a direction dependent filter on the isotropic measure of violation. Using this filtering method, a turbulent flow emerges due to fast increasing forces when the comfort zone diagonally behind the agent is violated. This violation causes the agent to rotate, however the comfort zone also rotates, increasing the violation. Eventually the boundary interaction force is sufficiently large to cancel this rotation. However, the turbulent flow has already been arisen. Hence, a different interaction causing less rotation is required.

Although the appropriate interactions are not found, the social force model has shown its potential for autonomous driving. With the social force model it is possible to let agents merge based on local interactions without using communication, while even improving the flow through a road narrowing.

Contents

List of Figures

List of Tables

Nomenclature

Accents

$\bar{}$	nominal
$\hat{}$	most effective
	(none) expressed in fixed world frame
$\tilde{}$	expressed in agent frame

Coordinates

x	x-coordinate
y	y-coordinate

Signals

ω	rotation speed
θ	orientation
a	acceleration
v	speed

Environment parameters

α	road narrowing tuning parameter
β	road narrowing tuning parameter
w_ℓ	lane width

Functions

Ψ	smoothing function expressed in the fixed world frame
ψ	1D bump function
$\tilde{\Psi}$	2D bump function expressed in the agent frame
Υ	Interaction function
g	violation
I	indicator function

Sets

$\mathbb{N}$	set of all natural numbers

$\mathbb{R}$	set of all real numbers
$\mathcal{V}$	agent set
$\mathcal{W}$	set describing obstacle
$\mathfrak{C}$	set describing comfort zone
$\mathbf{e}$	frame

Comfort zone parameters

ℓ	total comfort zone length
ℓ_b	comfort zone length behind the agent
ℓ_f	comfort zone length in front of the agent
ξ	smoothing factor
h	headway time
r	comfort zone radius
w_c	comfort zone width

Interaction parameters

γ	quadratic speed regulation constant
κ	tangential force constant
τ	characteristic time constant
k	normal force constant
m	mass
$v^{\max}$	maximum speed

Subscripts

b	back
f	front
i	agent index number
j	alternative agent index number
n	total number of agents
W	obstacle index number

Superscript

c	desired cruise
d	desired

Measures

δ	throughput

CTF cycle time factor

σ stress

φ flow time

A area

d distance

t time

Vectors

a acceleration vector

d distance vector

f interaction force vector

g violation vector

n normal vector

p position vector

q state vector

t tangential vector

v velocity vector

z arbitrary vector

Chapter 1

Introduction

This chapter provides the background information and problem statement of this thesis. Starting with the current (increasing) traffic problems and their causes. All these problems have one common solution: automation. While discussing different automation solutions, a common shortcoming is detected. This results in the problem statement of this thesis: create a control strategy for autonomous (highway) driving based on interaction rules, where the desired (collective) behavior emerges from these interaction rules. Next to that, the report outline is presented.

1.1 Background

Since 2013, traffic on the Dutch road has increased continuously [1], leading to longer travel times. In January and February 2017, the traffic-jam-weighting[1] has increased by 18% compared to 2016 [2]. The traffic-jam-weighting has increased slightly over the whole Dutch main road and not only at the top 10 traffic jam locations [1].

The overall cause of traffic jams is due to high intensity (67%) [1], however the problem underneath is not specified in this study. Research has classified the traffic jam causes at the top 15 traffic jam locations in 2011 which are: incident traffic jams (7%); shockwave traffic jams (22%); and infrastructural traffic jams (71%) [3].

Incident traffic jams can arise everywhere at any time. The cause of an incident traffic jam can be everything, such as road works, car crashes, weather and so on.

Shockwave traffic jams occur for no apparent reason. If speed fluctuations of a vehicle are amplified by the succeeding vehicles, a shockwave of continuously increased braking is caused. Eventually a vehicle comes to a standstill, resulting in a traffic jam. This behavior is (often) caused by too much traffic or erratic driving behavior.

Infrastructural traffic jams arise when the amount of traffic exceeds the road capacity. This is often the case during rush hours at locations where the number of lanes is reduced (i.e. road narrowings and entrance lanes).

1.2 Solutions to traffic problems

Since traffic jams have a large economic and environmental costs, people are constantly trying to find solutions to reduce (the effect of) traffic jams. Car manufacturers are trying to increase the reliability of their products and apply predictive maintenance to decrease the number of cars with car trouble at the side of the road. They also increase the safety (e.g. avoiding car crashes) by adding systems such as autonomous emergency braking and lane keeping assist. Furthermore, the Dutch roads are maintained well to

[1] traffic-jam-weight = length of the traffic jam in kilometers times the jam duration in minutes.

avoid unplanned road/lane closures. However, incident traffic jams cannot be overcome since incidents will always happen. Even though incidents cannot be avoided, they are currently the smallest cause of traffic jams.

A larger problem are shockwave traffic jams, which are currently tackled by two different methods. The first method is to provide drivers with speed information based on traffic ahead. If drivers react appropriately to the provided speed information, speed fluctuations are limited, a shockwave traffic jam is avoided. The speed information can be provided via the road side with dynamic route information panels (DRIPs) [4]. In addition, with the current state of technology the "grid" can be reduced by providing in-car information (e.g. via mobile phone apps) and also provide the global system with more data [5].

The second method to avoid shockwave traffic jams is by automation. By providing speed information to the user, it is assumed that drivers notice the speed information and react accordingly. However, this cannot be guaranteed. By applying automation, the desired behavior can be guaranteed. This could be done by implementing it in driver assistance systems such as adaptive cruise control. Most of today's luxury vehicles are equipped with adaptive cruise control (ACC), which is a cruise control (CC) system that automatically adjusts the speed to maintain a safe distance from vehicles ahead. However, ACC systems are merely focused on driving comfort and are not designed to damp shockwaves [6]. Although it is possible to damp shockwaves with ACC systems, a relatively large following distance is required [6, 7]. The damping performance can be increased by applying vehicle-to-vehicle communication. Here a vehicle communicates its acceleration to its successor such that it can be taken into account before measuring it. This ACC with feedforward by means of communication is called cooperative adaptive cruise control (CACC). Applying CACC, a headway-time of 0.7 seconds has proven to damp the shockwave [7], this is significantly less than with ACC. Therefore, Europe's truck manufacturers created a detailed timeline of steps leading up to the introduction of CACC on Europe's highways before 2025 [8]. Hence it is assumable that in the near future the effect of shockwaves will be reduced, resulting in less shockwave traffic jams.

The most common traffic jams are infrastructural traffic jams, which are also the hardest to prevent. These traffic jams occur when the road's capacity is exceeded. Two obvious solutions are adding road capacitance (e.g. add more lanes) or decrease traffic (e.g. avoiding rush hour or create alternative routes). However, the Braess Paradox [9] states that adding capacitance to a network can result in a decrease of overall performance. Hence, these solutions can have the opposite effect and are not future-proof since the amount of traffic keeps constantly increasing.

A third solution can be found when comparing traffic driving through a road narrowing with fluid (laminar) flowing through a bottleneck. These two scenarios are very similar see Figure 1.1.

To maintain a constant fluid flow, the law of conservation of mass must hold

$$\rho_1 A_1 v_1 \Delta t = \rho_2 A_2 v_2 \Delta t$$

with density ρ_i; area A_i; speed v_i; and the elapsed time Δt. A constant flow without buffering effect is obtained if this relationship holds for $\Delta t \to 0$. Hence, the speed and density (inter-vehicular distance) before and after the road narrowing should change accordingly.

To increase the speed and/or decrease the inter-vehicular distance after the road narrowing, without reducing safety is (almost) not possible for human drivers. Since humans have a relatively long reaction time compared to automated systems, the inter-vehicular distance can be (safely) decreased by means of automation. It has been proven that CACC can decrease the inter-vehicular distance while maintaining a safe distance to

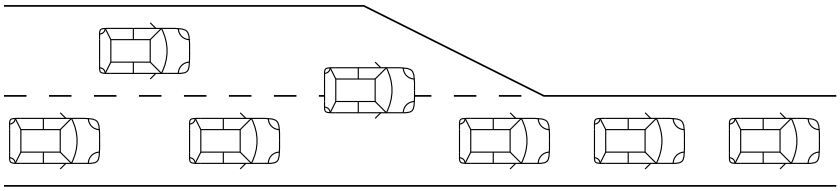

(a) Traffic driving through a road narrowing.

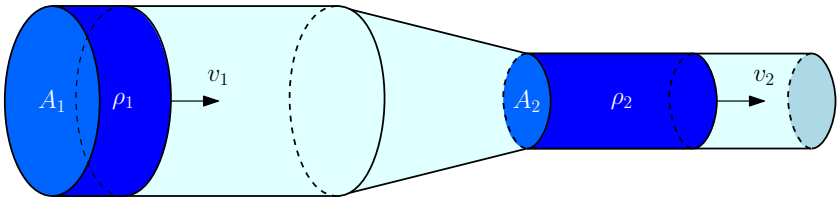

(b) Fluid flowing through a bottleneck.

Figure 1.1: Analogy between traffic driving through (a) a road narrowing and (b) fluid flowing through a bottleneck.

its predecessor. Furthermore, CACC has the communication available to "hear" what is "happening" downstream and react accordingly. To solve the infrastructural traffic jams at road narrowings and entrance lances, researchers explored the possibilities to automate the merging procedure while driving with CACC as explained in the next paragraph.

A merging protocol has been tested during the Grand Cooperative Driving Challenge 2016 [10]. The goal of the Grand Cooperative Driving Challenge (GCDC) is to accelerate the introduction of cooperative and automated vehicles in every day traffic. To do so, the GCDC 2016 had two challenges: cooperative platoon merge; and cooperative intersection passing. In the cooperative platoon merging scenario, two platoons (A & B) are required to merge. During the challenge, the merging protocol of Semsar-Kazerooni et al. [11] has been tested. The protocol is elaborated below (see Figure 1.2): (i) the platoons are aligned, the speeds are synchronized; (ii) platoon B is pairing up to platoon A, based on the closest neighbor; (iii) platoon A is pairing up to platoon B; (iv) cars start to make gaps such that the paired vehicle has enough space to merge in between; (v) when the gaps are ready, the platoon merges and a new platoon has been formed.

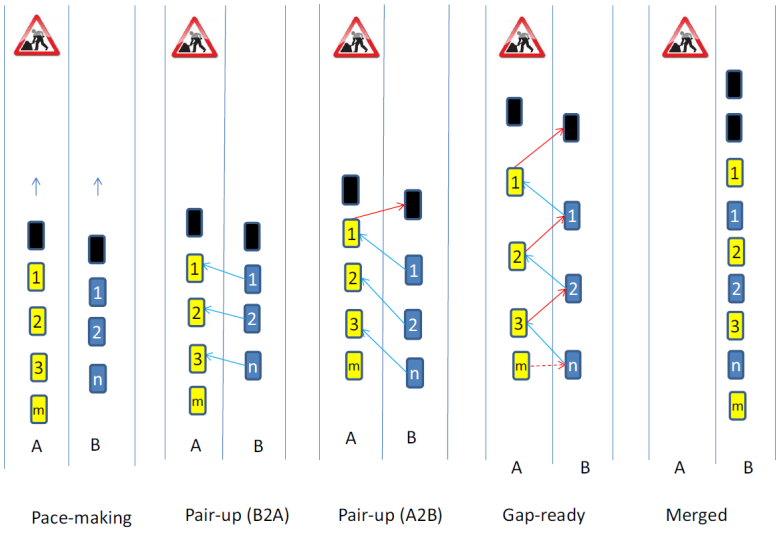

Figure 1.2: The platoon merging protocol as proposed by Semsar-Kazerooni et al. [11].

The drawback of this CACC merging protocol is that it lacks the ability to adapt to scenarios where a limit amount of space and/or time is available (i.e. robustness), since most steps occur simultaneously for all vehicles. Hence, the proposed protocol is not suitable to use in dense road traffic with many platoon members and/or limit space and time due to its stepwise nature.

A new merging procedure is currently developed [12] solving some of the flaws. However, this new merging solution is still only applicable in certain scenarios and also requires communication.

The (extensive) use of communication is not desired since the current bandwidth is (mostly) required for the working of CACC. Nevertheless, a scenario where the communication malfunctions causes a problem since the vehicles will be not able to merge. The requirement that all vehicles should be equipped with (working) communication modules is very restricting.

To reduce (or even solve) the infrastructural traffic jam problem, a method that changes the speed and inter-vehicular distance without using stepwise protocols and communication is required. Since most infrastructural traffic jams occur at road narrowings, merging is also required. Hence, an autonomous (highway) driving system is required. Therefore, the goal of this thesis is to find a new solution approach for autonomous (highway) driving without the need of communication and stepwise protocols.

This new solution approach can have a wide range of applications (besides traffic), e.g. autonomous transportation tasks in warehouses, harbors, factories etc.. A current solution for autonomous transportation is using a supervisory system which assigns a reference path with a desired velocity profile to each agent. However, this will not guarantee collision-free movements (e.g. due to disturbances), therefore a tracking controller with collision avoidance as in [13] can be used. This solution requires a non-equal priority assignment for each agent such that the system does not end in a deadlock. Consequently requiring communication or general knowledge of each agent's priority, which is impractical for an increasing number of agents in a dynamic environment. Hence, the restriction on communication and stepwise protocols is also applicable for a wider range applications, emphasizing its importance.

1.3 Social interaction forces

To find a suitable merging strategy, nature is consulted. In nature there are many examples of collective behavior: swarms of bees; flocks of birds; herds of sheep; and crowds of pedestrians. The collective behavior of swarms is often self-organized. This means that collective behavior emerges from the underlaying (local) interaction rules and are not externally planned or prescribed [14–16].

The desired merging behavior can be found in human crowds. We (humans) can walk through a bottleneck scenario and merge without colliding (under normal conditions). The passing time distributions are equally spread [17], hence nobody has to wait extremely long before merging and passing through the bottleneck.

Such collective movements are often analyzed and predicted by modeling individuals with virtual physics [18, 19]. A well-known (and proven) model to study crowd dynamics is the social force model of Helbing et al. [17, 20, 21]. The social force model describes the behavior of an individual pedestrian by a superposition of generalized forces reflecting motivation and environmental influences.

The interaction rules obtained from the social force model are also successfully applied to create an autonomous navigation controller for differential wheeled mobile robots [22]. Each agent (mobile robot) has a comfort zone which creates a repulsive force when it is violated by an environmental obstacle or another agent's comfort zone, therefore avoiding

collisions. An attractive force drives the agent to its target location. Simulations and experiments show that this navigation controller can drive six mobile robots to different target locations without colliding in various scenery (including a bottleneck scenario) [22].

From other research it is known that the dynamics of an individual are very important to the (collective) behavior. A flock of birds can be modeled using three interaction rules: attraction, alignment and avoidance [23]. However, a school of fish can be modeled using the same three interaction rules but show a different collective behavior [16]. The difference in collective behavior is subject to the dynamics of the individuals. A fish is more likely to slow down to avoid collisions while a bird changes its orientation [16], resulting in a different collective motion.

Thus, to find or create a suitable merging strategy, the interaction rules from the social force model can be a good source of inspiration. Although the dynamics of the individual play an important role and should be taken into account.

1.4 Artificial potential fields

Another common method to drive robots through a dynamic environment is by employing artificial potential fields. Many applications of artificial potential field can be found in the field of swarm robotics [18, 19, 24–28]. Swarm robotics is "the study of how large numbers of relatively simple physically embodied agents can be designed such that a desired collective behavior emerges from the local interactions among agents and between the agents and the environment." [29]. Typically the used potential function $U(q) := U_{\text{att}}(q) + U_{\text{rep}}(q)$ includes attraction $U_{\text{att}}(q)$ towards its goal and repulsion $U_{\text{rep}}(q)$ from all obstacles in the workspace [30]. The desired motion from any given pose q can be determined by the gradient descent $\dot{q} := -\alpha \nabla U(q)$.

An example of an artificial potential field for highway driving with collision avoidance in a full two-dimensional field is created by Wolf and Burdick [31]. Additionally, it includes implicit decision making, whether to pass slow obstacles or stay behind them. A geometric shape (rectangle) is created around all other agents such that the lateral dimensions can differ from the longitudinal dimension. A wedge is added to the back of the other agents to provoke lane changing (see Figure 1.3). The agent should only change lane if the speed difference is sufficiently large, therefore the dimensions of the wedge is based on the speed difference between the two agents. A larger speed difference implies a longer wedge.

The work of Wolf and Burdick differs from other research since they created a potential field in a two-dimensional field with implicit decision making. In other research the potential functions for longitudinal and/or lateral control are derived separately, subsequently combined to create a two-dimensional field [32–36]. Even merging protocols for the longitudinal direction are created using artificial potential functions [12], however they still contain the stepwise protocol. Nonetheless, the artificial potential functions are very intuitive and a priori based, therefore they are only valid for very specific situations.

The generalized forces of different social interaction models [16, 17, 20, 21, 23] define the desired motion, which can be seen as the gradient of an artificial potential function. Hence, the social force model also creates a two-dimensional artificial potential field by defining the gradient instead of the potential function. The social force model of Helbing et al. [21] distinguishes itself from the other potential fields since it takes the other agent's comfort zone into account, therefore both agents experience an interaction force. Due to the mutual interaction, the agents exhibited a more "social" behavior since the other agent's preferences are considered.

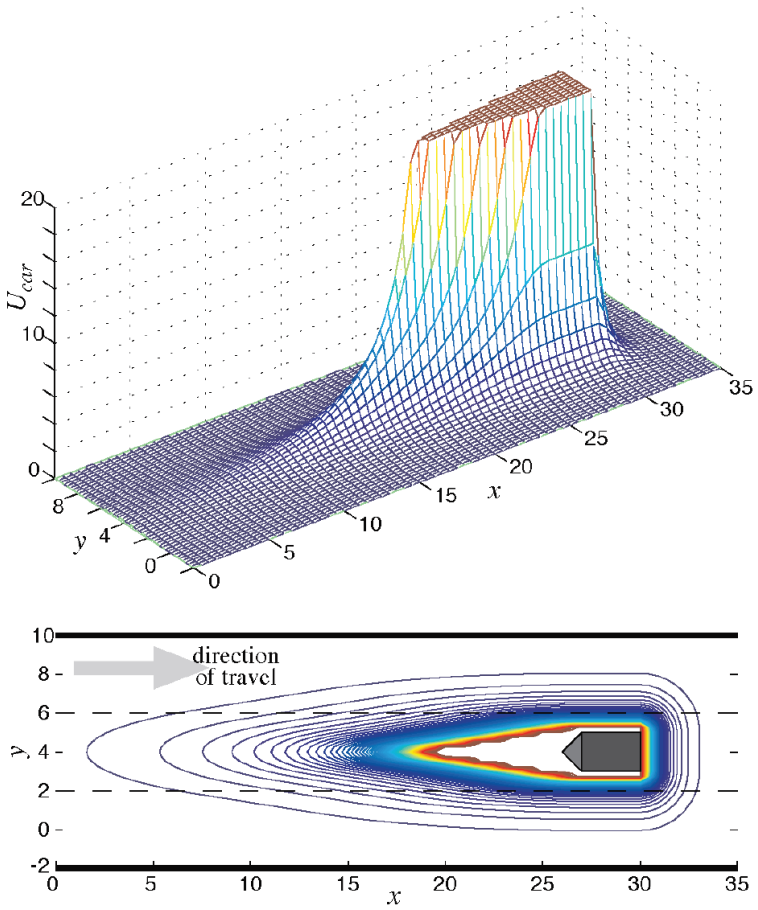

Figure 1.3: Visualization of the car potential function designed by Wolf and Burdick [31].

1.5 Problem statement

The main short coming in the current design of autonomous driving controllers and merging strategies is the use of stepwise protocols and their application in very specific situations. Furthermore, the development of these control strategies merely focuses on microscopic behavior and not on the macroscopic effect. Therefore, the goal of this thesis is to **create a control strategy for autonomous (highway) driving based on interaction rules, where the desired (collective) behavior emerges from these interaction rules.** Here (highway) driving includes: lane keeping; driving at a desired speed or (safe) distance to its predecessor; and merging.

The control strategy should be able to work without communication with other agents or its environment since communication is a very restrictive requirement. This means that the available signals are based on data obtained from (local) measurements. Thereby assuming that the following information is available without time delays:

- (relative) position;
- (relative) orientation;
- (relative) velocity.

Setting highway driving including merging as a goal brings several challenges. The first challenge is to create the desired collective behavior based on local interaction rules. Since it is known that the dynamics of an individual have a great influence on the collective behavior, the constraints of a vehicle should be taken into account. Hence, a representative vehicle model should be used.

The second challenge is to include geometry in the control strategy. Geometry is desired since vehicles drive on different lanes, consequently the lateral distance may be smaller than the longitudinal distance. E.g. driving one meter to the side of another car is more acceptable than following one meter behind. However, in most research the Euclidean distance to another agent (assumed to be a point) is used to determine the magnitude of the reaction force. The Euclidean distance is isotropic (direction independent), which is not desired in this scenario. Therefore, an alternative method to determine the magnitude of the interaction force is required.

The last challenge is including a spacing policy. The inter-vehicle distance should be subject to the speed such that the minimum amount of road is used while guaranteeing safety. Thus, in analogy to the fluid model, the density should be speed depended.

To test and measure the macroscopic performance of the new control strategy, a road narrowing as shown in Figure 1.4 is used as design and test case. Initially the road starts with two lanes (section 1) and will be reduced (section $1 \rightarrow 2$) to a road with one lane (section 2). Thus, this scenario includes: lane keeping; driving at a desired speed or (safe) distance to its predecessor; and merging.

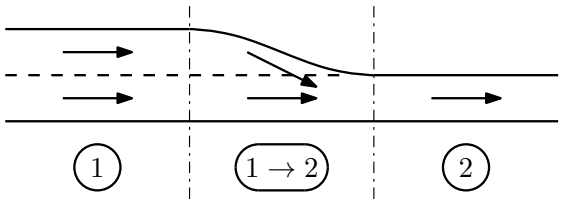

Figure 1.4: The selected scenario, a road narrowing from (initially) two lanes to one lane.

1.6 Solution approach

To find a suitable solution approach, the features of the earlier mentioned automation solutions are summarized in Table 1.1.

Since the goal is to let the desired (collective) behavior emerge from the interaction rules, the social force model is chosen as the framework to design the interaction rules in. The choice for the social force model may be counter intuitive since most features have already been implemented in artificial potential fields. However, the greatest advantage of the social force model is that the collective behavior is already known since it is used to study crowd dynamics. From [17] it is known that no agent has to wait extremely long before merging and passing through the bottleneck. Thus, the agents exhibit a "social" behavior by sharing discomfort, which is a desired feature for the new control strategy.d Furthermore, the social force model should have the same possibilities to embed the features as artificial potential fields since the generalized social force is the gradient of such a field. Hence, the required features of the other methods (representative vehicle model; spacing policy; and agent geometry) can be added to the social force model.

Since CACC is only defined in the one-dimensional plane it is nontrivial to apply it in the full two-dimensional field. Furthermore, CACC is merely focused on damping shockwaves by improving the performance of ACC. Therefore, CACC is not a good starting point for autonomous driving but might be implemented in a later stage to improve performance.

Table 1.1: Feature overview of the social force model (SFM), artificial potential fields (APF), cooperative adaptive cruise control (CACC) and adaptive cruise control (ACC).

Feature	**SFM**	**APF**	**CACC**	**ACC**
Works in the (full) 2D-field	✓	✓	✗	✗
Social / cooperative behavior	✓	✗	✓	✗
Contains representative vehicle model	✗/✓	✓	✗	✗
Efficient road usage (spacing policy)	✗	✓	✓	✓
Damping shockwaves	✗	✗/✓	✓	✗/✓
Implicit decision making	✓	✓	✗	✗
Does not require communication	✓	✓	✗	✓
Including agent geometry	✗	✓	✗	✗

1.7 Report outline

The rest of this thesis is organized as follows. In Chapter 2 the general methodology is introduced, covering the social force model and macroscopic performance measurements. It is followed by Chapter 3, where the interactions are derived based on the social force model of Helbing et al. and some of the required features are added. These newly designed interactions are tested by means of simulations. The simulation method and corresponding outcomes are discussed in Chapter 4. Based on these results, Chapter 5 discuses alternative interaction designs. Finally, Chapter 6 provides the conclusions and recommendations of this thesis.

Chapter 2

General methodology

This chapter will first cover the multi-agent model, starting with the details of the used scenario: the road narrowing. Thereafter, the multi-agent model is discussed. The multi-agent model consists of two parts, namely the agent kinematics and the interactions. The differential wheeled mobile robots, considered as agents, are represented by the well-known unicycle kinematics. In addition the interaction frame work is defined, followed by a general form of the inter-agent interactions and environmental interactions. The first part is concluded with a model overview.

The second part defines the measurements to indicate the macroscopic performance of the control strategy. The four measurements which are defined are: flow time; cycle time factor; throughput; and stress. Furthermore, the definition of the $\mathcal{L}_2$-norm is given.

2.1 The multi-agent model

The goal is to create a control strategy for autonomous (highway) driving based on interaction rules. The desired collective behavior should emerge from the interactions between agents; and agents and their environment. Hence, the used scenario is of great importance. Therefore, the geometric problem description will be covered first. It is followed by the agent kinematics; the interaction framework; a general form of the interactions; and a model overview.

2.1.1 Geometric problem description

The lane reduction scenario is modeled as shown in Figure 2.1. Initially the road starts with two lanes, where each lane has a width w_ℓ. Eventually the upper lane is removed and only the lower lane remains.

Initially, there are n agents equally distributed over the two lanes with a longitudinal inter-agent distance d_0. Each agent $i \in \mathcal{V} := \{1, \ldots, n\}$ has an orientation θ_i, position $\mathbf{p}_i := \begin{pmatrix} x_i & y_i \end{pmatrix}$ and velocity $\mathbf{v}_i := \begin{pmatrix} \dot{x}_i & \dot{y}_i \end{pmatrix}$ with respect to the fixed world frame $\mathbf{e}^0$.

The environment (i.e. road-layout) is constructed out of different obstacles. The geometry and location of obstacle W is described by the set $\mathcal{W}_W \subsetneq \mathbb{R}^2$. To create the road lay-out, three different obstacles are defined: the lower road boundary; the upper road boundary reducing the number of lanes; and the lane separation.

The set representing the lower road boundary

$$\mathcal{W}_1 := \left\{ \mathbf{z} \in \mathbb{R}^2 \mid y = c \right\}$$

describes a straight line. Here $\mathbf{z} := x e_1^0 + y e_2^0 = \begin{pmatrix} x & y \end{pmatrix} \mathbf{e}^0$ and c is an arbitrary constant indicating the location of the lower road boundary with respect to the fixed world frame.

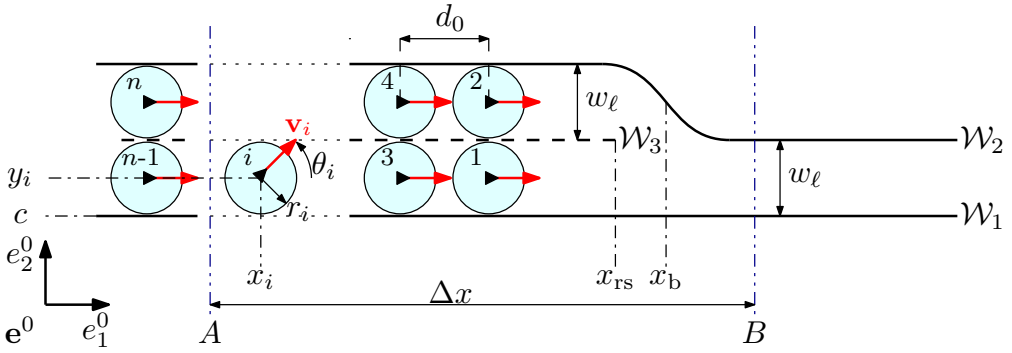

Figure 2.1: Model of the scenario.

The constant c is only used for visualization purposes and has no effect on the overall dynamics.

The obstacle, describing a sigmoid, represents the upper road boundary which reduces the number of lanes

$$\mathcal{W}_2 := \left\{ \mathbf{z} \in \mathbb{R}^2 \mid y = c + 2w_\ell - \frac{w_\ell}{\left(1 + e^{-\alpha(x - x_{\text{b}})}\right)^{\frac{1}{\beta}}} \right\},$$

with lane width w_ℓ; the x-value of the sigmoid's midpoint x_{b} (see Figure 2.1); and tuning parameters α and β.

The last obstacle set describes the lane separation, which is only present in a certain region

$$\mathcal{W}_3 = \left\{ \mathbf{z} \in \mathbb{R}^2 \mid x \leq x_{\text{rs}},\ y = c + w_\ell \right\}.$$

The numerical parameters for the boundaries are presented in Table 2.1. The parameters are chosen such that the center of road narrowing is set at the origin of the fixed world frame. This only has a visual benefit and does not affect the system dynamics. Furthermore, the parameters are based on the dimensions of the e-puck [37] and corresponding comfort zone as used in the work of Rodriguez-Angeles et al. [22].

Table 2.1: The used numerical values for the boundary parameters.

Parameter	c	w_ℓ	α	β	x_{b}	x_{rs}
Value	-0.1	0.1	1	0.2	0	-0.5

2.1.2 Agent kinematics

Since the agent dynamics can have a great influence on the collective behavior it is important to take them into account. The agent dynamics can be included by modeling the agent as a point mass with a certain damping $m\ddot{q} + d\dot{q} = F$, where q represents the agent's pose. However, this damping term d is vehicle depended and has a great influence on the overall performance. Another possibility to take the agent dynamics into account is by including the no lateral slip condition (nonholonomic constraint), which vehicles often possess, into the agent kinematics.

Each agent is considered as a differential wheeled mobile robot, represented by the kinematic model of a unicycle (2.1). On one hand the kinematic bicycle model would have been a more intuitive choice for modeling a vehicle since the focus of the application is on traffic. On the other hand, the social force model has been successfully applied on a differential wheeled mobile robot [22], which is represented by the unicycle kinematics. Nevertheless, the unicycle and bicycle model possess the same nonholonomic constraint.

To follow up on the work in [22] the unicycle kinematics are chosen, with the advantage that it could be tested on the e-puck mobile robots.

The unicycle model

$$\begin{aligned} \dot{x_i} &= v_i \cos(\theta_i) \\ \dot{y_i} &= v_i \sin(\theta_i) \\ \dot{\theta_i} &= \omega_i \end{aligned} \tag{2.1}$$

has longitudinal speed v_i and rotation speed ω_i as control inputs.

2.1.3 Interaction framework

The interaction framework is based on the social force model of Helbing et al. [17, 20, 21], used to study crowd dynamics. The social force model describes the behavior of an individual pedestrian by a superposition of generalized forces reflecting motivation and environmental influences. In the work of Rodriguez-Angeles et al. [22] the generalized forces of the social force model as in [21] defines the desired motion.

For greater possibilities, a more general interaction framework is derived based on the work in [21, 22]. The desired acceleration (i.e. motion) of agent i is described by

$$m_i \mathbf{a}_i^d := m_i \left(1 + \gamma_i \frac{||v_i^c \mathbf{e}^d - \mathbf{v}_i||}{\tau_i}\right) \frac{v_i^c \mathbf{e}^d - \mathbf{v}_i}{\tau_i} + \sum_{i(\neq j)} \mathbf{f}_{ij} + \sum_W \mathbf{f}_{iW}. \tag{2.2}$$

Here $\mathbf{v}_i := \begin{pmatrix} \dot{x}_i & \dot{y}_i \end{pmatrix}$ is the velocity vector and $\mathbf{a}_i^d := \begin{pmatrix} a_{i,x}^d & a_{i,y}^d \end{pmatrix}$ the desired acceleration vector. The first right hand term in (2.2) regulates the agent to its desired cruise speed v_i^c in the desired direction $\mathbf{e}_i^d := \begin{pmatrix} 1 & 0 \end{pmatrix}$, with the characteristic time constant τ_i. Here $||\cdot||$ denotes the Euclidean-norm. The constant gain γ_i makes $\frac{||v_i^c \mathbf{e}^d - \mathbf{v}_i||}{\tau_i}$ dimensions less and is called the "quadratic speed regulation term". With $\gamma_i = 0$ the model is equal to the model as presented in [21, 22]. This quadratic speed regulation term is introduced to compensate for the effect of the spacing policy, which is covered in Section 3.2.3.

The reaction force between agent i and other agent $j \in \mathcal{V}$ is represented by the vector $\mathbf{f}_{ij} \in \mathbb{R}^2$. The reaction force between agent i and the environmental obstacle W (e.g. road boundaries) is given by the vector $\mathbf{f}_{iW} \in \mathbb{R}^2$. All these vectors are expressed with respect to the fixed world frame $\mathbf{e}^0$ as shown in Figure 2.1. The general form of these interaction forces is elaborated below and will be specified in Chapter 3.

Inter-agent interactions

The inter-agent interaction force $\mathbf{f}_{ij}$ is defined as

$$\mathbf{f}_{ij} := \Big(\Upsilon_{ij}(\mathbf{q}_{ij}) g_{ij}(\mathbf{q}_{ij})\Big)\Big(k_i \mathbf{n}_{ij} + \kappa_i \Delta v_{ji}^t \mathbf{t}_{ij}\Big), \tag{2.3}$$

where $\mathbf{q}_{ij} := \begin{pmatrix} \mathbf{p}_i & \mathbf{p}_j & \mathbf{v}_i & \mathbf{v}_j \end{pmatrix} \in \mathcal{Q}_{ij} := \{\mathbb{R}^2 \times \mathbb{R}^2 \times \mathbb{R}^2 \times \mathbb{R}^2\}$.

The interaction function $\Upsilon : \mathbb{R}^2 \times \mathbb{R}^2 \times \mathbb{R}^2 \times \mathbb{R}^2 \to [0, 1]$ indicates if there is interaction between agent i and j. In general, if the comfort zone of agent i is violated by agent j the function $\Upsilon_{ij} = 1$, otherwise $\Upsilon_{ij} = 0$. To reduce the stiffness of the multi-agent problem, the interaction function can be smooth such that the interaction force is gradually increasing. The velocity of both agents is an argument of Υ_{ij} since the comfort zone of the agents can be speed depending (due to the application of the spacing policy).

The violation function $g_{ij} : \mathbb{R}^2 \times \mathbb{R}^2 \times \mathbb{R}^2 \times \mathbb{R}^2 \to \mathbb{R}$ determines the weighting of the applied interaction force based on the comfort zone violation. Since the comfort

zones can depend on the speed, the velocities are also an argument of this function. To only allow repulsive forces due to comfort zone violation, the violation function must be semi-positive if the interaction function is non-zero

$$g_{ij}(\mathbf{q}_{ij}) \geq 0 \quad \forall\, \mathbf{q}_{ij} \in \left\{ \mathcal{Q}_{ij} \mid \Upsilon_{ij}(\mathbf{q}_{ij}) \neq 0 \right\}.$$

The amplitude and direction of the interaction force are determined by the constants k_i, κ_i. The normal vector pointing from agent j to i is $\mathbf{n}_{ij} := \begin{pmatrix} n_{ij,x} & n_{ij,y} \end{pmatrix}$ and the tangential vector $\mathbf{t}_{ij} := \begin{pmatrix} -n_{ij,y} & n_{ij,x} \end{pmatrix}$. The tangential velocity difference is given by $\Delta v_{ji}^t := (\mathbf{v}_j - \mathbf{v}_i)\mathbf{t}_{ij}$.

Remark. *This is a more general definition of the inter-agent force than in the work of Helbing [21] and Rodriguez-Angeles [22], with the additional restriction that in only allows repulsive forces. However, the working principle is similar to the work of Rodriguez-Angeles [22] and the same results can be achieved.*

Environmental interactions

The environmental interaction forces are very similar to the inter-agent interaction forces. If the comfort zone of agent i is violated by an environmental obstacle W, the term $\mathbf{f}_{iW}$ generates a repulsive interaction force

$$\mathbf{f}_{iW} := \hat{k}_W \Big(\Upsilon_{iW}(\mathbf{q}_{iW}, \mathcal{W}_W) g_{iW}(\mathbf{q}_{iW}, \mathcal{W}_W) \Big) \Big(k_i \mathbf{n}_{iW} + \kappa_i (\mathbf{v}_i \cdot \mathbf{t}_{iW}) \mathbf{t}_{iW} \Big), \tag{2.4}$$

where $(\mathbf{q}_i) := \begin{pmatrix} \mathbf{p}_i & \mathbf{v}_i, \end{pmatrix} \in \mathcal{Q}_i := \{\mathbb{R}^2 \times \mathbb{R}^2\}$. All functions are like the functions defined at the inter-agent interactions, however agent j is replaced by obstacle W. The term $\Delta v_{ji}^t \mathbf{t}_{ij}$ from (2.3) is similar to $(\mathbf{v}_i \cdot \mathbf{t}_{iW})\mathbf{t}_{iW}$ since an environmental obstacle cannot move. The tangential speed difference is thus the agents' own speed tangential to the obstacle. Furthermore, there is an additional parameter $\hat{k}_W$ who's value depends on the obstacle type.

There are two types of obstacles, road edges (boundaries) and lane divisions. The goal of the road edge is to keep the agents on the road. Therefore, the interaction force needs to be sufficiently large with respect to the inter-agents interaction forces. Assuming that a maximum of 3 agents can try to push another agent of the road (one from each side), the road edge should deliver a sufficiently large force. Choosing $\hat{k}_W = 4$ if obstacle W is a road edge, the boundary interaction force is significantly larger than the inter-agent interaction forces.

The goal of the lane division is to keep agents in their lane under "normal" circumstances. However, under certain conditions, e.g. if the lane is jammed and the adjunct lane is not, the agent should be able to change lane. To achieve this, the environmental force should be significantly lower than the inter-agent interaction force. Therefore, $\hat{k}_W = \frac{1}{4}$ if obstacle W is a lane division.

Linking the social force model to the kinematic model

The social force model (2.2) generates a generalized force for agent i. Via Newton's second law, this can be transformed to the desired acceleration $\mathbf{a}_i^d$. However, the desired acceleration cannot be directly used as input for the unicycle kinematics due to the nonholonomic constraint. The inputs of the unicycle model are the forward speed v_i and rotation speed ω_i. Therefore, the challenge is to turn the desired acceleration into appropriate control inputs for the kinematic model.

Dynamic feedback linearization as in [38] cannot be used since it does not allow agents to stand still ($v_i \neq 0$), while coming to a standstill is very common in traffic jams. In

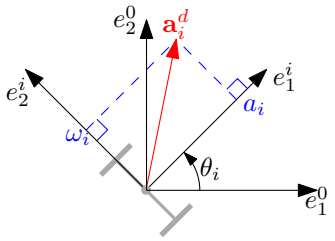

Figure 2.2: The projection method visualized.

the work of Rodriguez-Angeles et al. [22], the nonholonomic constraint is rewritten to obtain these desired inputs. However, this strategy may result in unstable behavior, as shown in Section 4.2 and Appendix B. Therefore, a different strategy similar to the work of Tanner et al. [25] is created. A projection of the desired acceleration is taken on the current orientation of the unicycle (see Figure 2.2), resulting in a forward acceleration a_i and a rotation speed ω_i

$$\begin{pmatrix} a_i \\ \omega_i \end{pmatrix} := \begin{pmatrix} \cos(\theta_i) & \sin(\theta_i) \\ -\sin(\theta_i) & \cos(\theta_i) \end{pmatrix} \begin{pmatrix} a_{i,x}^d \\ a_{i,y}^d \end{pmatrix}. \tag{2.5}$$

The rotation speed is one of the inputs of the kinematic model and can be used directly. The other input, the forward velocity v_i, is obtained by integrating the forward acceleration

$$a_i =: \dot{v}_i.$$

Furthermore, the input v_i has a saturation limit such that the agent cannot move backward $v_i^{\min} = 0$ and has a maximum speed $v_i^{\max}$.

2.1.4 Model overview

By applying the projection method, a proper connection is made between the social force model and the unicycle kinematics. The output of the social force model, the desired acceleration, is translated by the projection method to a forward and rotation speed. Which are the inputs of the unicycle model, describing the agent's kinematics. Using the unicycle kinematics, an agent is considered to be a point mass with an orientation.

A complete overview is given in Figure 2.3, where all interactions between the different submodels are shown. The interactions take place within the dash-dotted line, which defines the gradient of the artificial potential function for each agent.

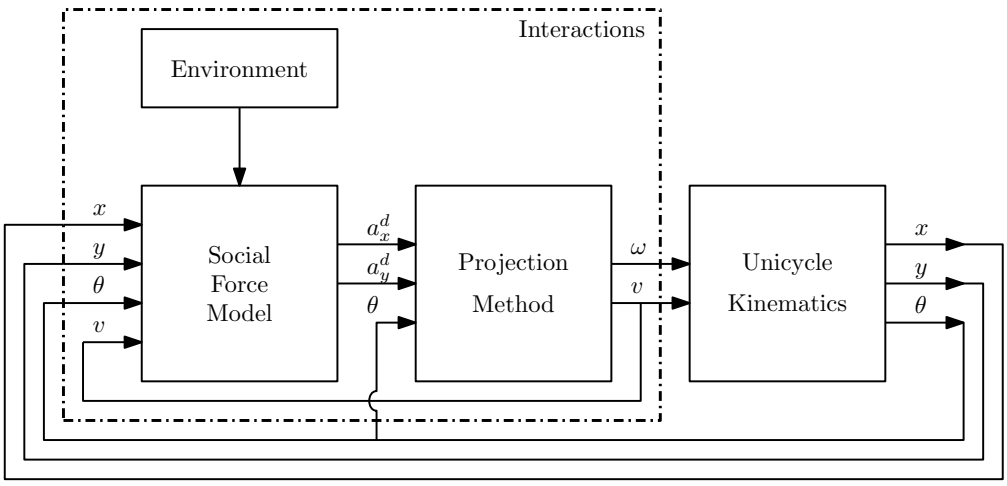

Figure 2.3: Composition of the complete mathematic model.

2.2 Measurements

The earlier discussed social force model describes the agents on a microscopic level. The goal is to design the microscopic interactions to provoke a certain macroscopic behavior, namely increasing the throughput of the road narrowing and fluent merging. The macroscopic performance of the collective behavior is hard to see when using a microscopic model. To state something about the collective behavior, measurements are required. Therefore, the following measures are introduced:

- flow time;
- cycle time factor;
- throughput;
- stress.

Furthermore, a definition of the used $\mathcal{L}_2$-norm is given.

2.2.1 Flow time

In literature the travel time, cycle time or flow time φ_i is often analyzed [39–42]. This are different names for the same measurement.

Definition 1. *The flow time is the time it takes for an agent to travel from line $x = A$ to line $x = B$ over a distance $\Delta x = |B - A|$.*

The lines $x = A$, $x = B$ and distance Δx are visualized in Figure 2.1. This measurement gives an indication about the average speed of an agent over the used interval.

2.2.2 Cycle time factor (CTF)

Analyzing the effect of different cruise speeds using the flow time distribution would be hard. Especially in the field of manufacturing systems, the cycle time factor (CTF) is used to analyze the effect of a parameter on the speed [43, 44]. The cycle time factor is determined by dividing the flow time by the nominal flow time[1]. The nominal flow time of an agent is determined by dividing the interval distance Δx by the desired (cruise) speed v_i^c.

Definition 2. *The cycle time factor is*

$$CTF_i := \frac{\varphi_i \cdot v_i^c}{\Delta x}.$$

Remark. *With this definition of the nominal flow time the effect of the road narrowing on the top lane agents is neglected (it is assumed that if the agent is alone in the system it would drive on the lane which is not removed).*

2.2.3 Throughput

Another common measure in literature to indicate performance is flow or throughput δ [39–45]. The throughput is measured by counting the number of agents ΔN passing a line $x = C$ during a certain time interval ΔT. The throughput at line $x = C$ is then determined by

$$\delta(x) = \frac{\Delta N}{\Delta T}$$

[1] The nominal flow time is the time it takes for an agent to pass through the road narrowing if it is the only agent present in the system.

with arbitrary constant C, where the unit of the throughput is agents per time unit.

However, this is not the appropriate measure to use when performing simulations with only a few agents. Therefore, the throughput measurement is redefined by taking the time it takes to let all agents pass a line, starting with the first agent.

Definition 3. *The throughput $\delta(x)$ in agents per second is*

$$\delta(x) := \frac{n}{t_2 - t_1},$$

where the time that the first agents passes the measurement line on position x is denoted as t_1, the time that the last agents passes this line is t_2 and the total number of agents passing the line is n.

2.2.4 Stress

The last measurement is the agent's stress. An agent can experience a different forces due to the inter-agent interactions. It is possible that these forces cancel each other out, however a slight disturbance could lead to a sudden change in the amplitude of the generalized force. To measure the possibility of the sudden change, denoted as "stress", the magnitude of the inter-agent forces is taken. The magnitude of the force is divided by the distance between the interacting agents since an agent close by has in general a larger effect on the dynamics than an agent far away.

Definition 4. *The total stress an agent experiences is*

$$\sigma_i := \sum_j \frac{||\boldsymbol{f}_{ij}||}{d_{ij}}.$$

Remark. *The unit of this agent stress is Newton per meter, while engineering stress is expressed as a pressure in Newton per square meter [46]. Hence, there is no (direct) relation between the agent stress and engineering stress.*

2.2.5 $\mathcal{L}_2$-norm

Besides the earlier defined measures for the macroscopic behavior, it can be interesting to determine the total energy of an agent specific signal e.g. the stress $\sigma_i(t)$ or rotation speed $\omega_i(t)$. The energy of a signal is determined by the $\mathcal{L}_2$-norm as defined in [47, 48].

Definition 5. *The $\mathcal{L}_2$-norm of a signal $z(t) = \begin{pmatrix} z_1(t) & z_2(t) & \dots & z_n(t) \end{pmatrix}$ is*

$$\begin{aligned} ||z(t)||_{\mathcal{L}_2} &:= \left(\int_0^\infty z^T(t) z(t) dt \right)^{\frac{1}{2}} \\ &= \left(\int_0^\infty ||z(t)||^2 dt \right)^{\frac{1}{2}}. \end{aligned}$$

Chapter 3

Interaction design

The general methodology covered in the previous chapter does not define the interactions. The interactions are depending on the definition of the interaction and violation function. In this chapter different interaction rules will be derived. First the interactions from the social force model as defined by Rodriguez-Angeles et al. [22] are discussed. Thereafter social-ACC is derived, which is based on the social force model as defined by Rodriguez-Angeles et al. but with a speed depending comfort zone size (i.e. spacing policy). The novelty in social-ACC is that the other agent's comfort zone is taken into account. The hypothesis is that this induces a more social behavior where agents make place for each other, resulting in a better flow through the road narrowing. To see the effect of social-ACC, an implementation of 2D-ACC has been made. This should reflect the working principle of ACC or more human-like driving. The expected working principles of social-ACC and 2D-ACC is shown in Figure 3.1.

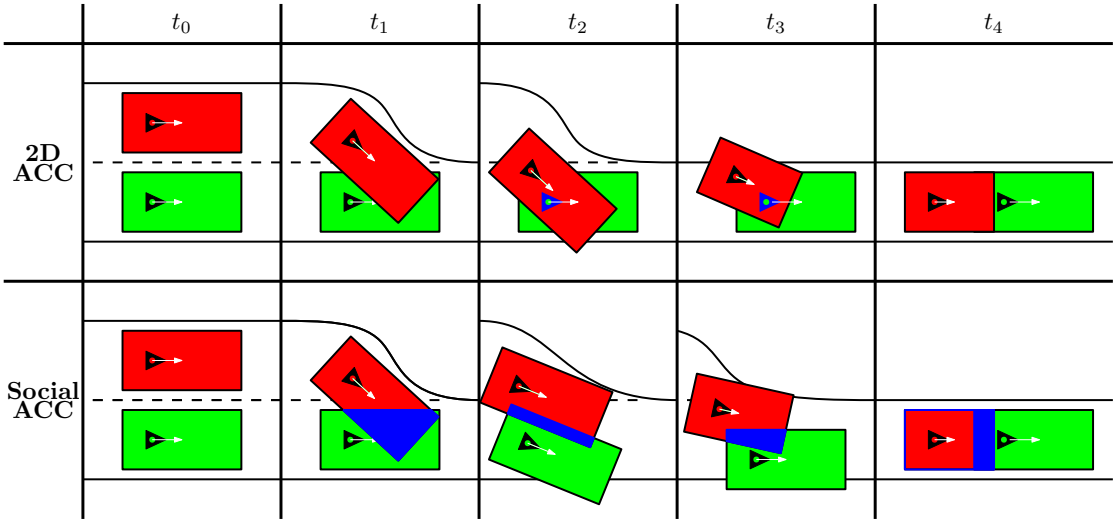

Figure 3.1: The hypothetical difference in working principle of 2D-ACC and social-ACC. With (top) 2D-ACC an agent only reacts when another agent is in its comfort zone, while (bottom) with social-ACC both agents interact if their comfort zones intersect.

3.1 Social force model by Helbing

The social force model by Helbing is characterized by the circular comfort zones, where the sizes are speed independent. An agent will experience a force if the comfort zone is violated by an obstacle or another agent's comfort zone. The interaction created by the

overlap of the two comfort zones is what makes the social force model "social" since it takes another agent's preference into account.

In the original model by Helbing, the tuning parameter γ_i does not exist, therefore it is set to 0. Hence, the desired motion of an agent is given by

$$m_i \mathbf{a}_i^d := m_i \frac{v_i^c \mathbf{e}^d - \mathbf{v}_i}{\tau_i} + \sum_{i(\neq j)} \mathbf{f}_{ij} + \sum_W \mathbf{f}_{iW}.$$

In the following subsections the inter-agent interaction force $\mathbf{f}_{ij}$ and the environmental interaction force $\mathbf{f}_{iW}$ will be specified.

3.1.1 Inter-agent interactions

Agent $i \in \mathcal{V}$ has a circular comfort zone with radius r_i. If for agent $j \in \{\mathcal{V} | i \neq j\}$ the comfort zone intersects the comfort zone of agent i, the interaction function becomes 1. The inter-agent interaction function Υ_{ij} is then defined by the inter-agent indicator function I_{ij}

$$\Upsilon_{ij} := I_{ij}.$$

The inter-agent indicator function $I_{ij} \in \{0, 1\}$ is defined as

$$I_{ij} := \begin{cases} 1 & \text{for } r_{ij} - d_{ij} \geq 0 \\ 0 & \text{otherwise} \end{cases} \tag{3.1}$$

with $r_{ij} := r_i + r_j$ and $d_{ij} := ||p_i - p_j||$.

The violation caused by another agent is the overlap of the two comfort zones

$$g_{ij} := \max\left(0, r_{ij} - d_{ij}\right), \tag{3.2}$$

visualized in Figure 3.2. A visualization of both functions in $\mathbb{R}^2$ is given in Figure 3.3.

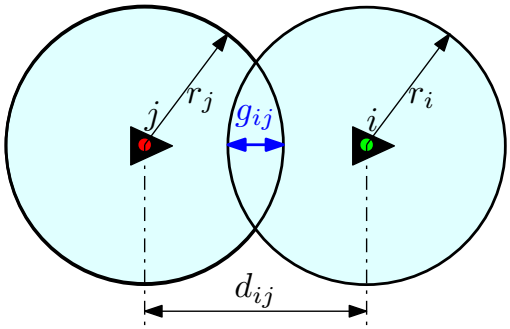

Figure 3.2: In the original social force model the amount of violation g_{ij} is measured as the overlap of two comfort zones.

3.1.2 Environmental interactions

The environmental interactions are very similar to the inter-agent interactions. However, an environmental obstacle does not have a comfort zone, therefore only the agent's comfort zone is used. If an obstacle W is inside the comfort zone of agent i, the comfort zone is violated and the interaction function becomes 1. The environmental interaction function Υ_{iW} is defined by the environmental indicator function I_{iW}

$$\Upsilon_{iW} := I_{iW}.$$

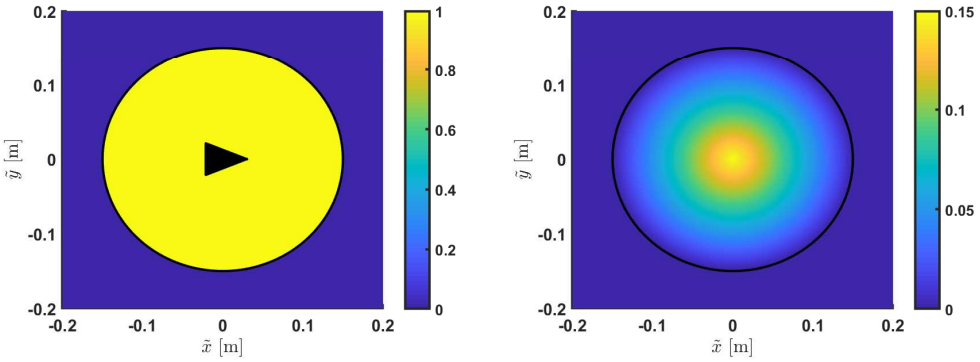

(a) $\Upsilon_{ij} := I_{ij}$ (b) g_{ij}

Figure 3.3: Individual inter-agent function visualization from the social force model by Helbing in the 2D-plane. (a) Interaction function and (b) violation function.

The environmental indicator function $I_{i,W} \in \{0, 1\}$ is defined as

$$I_{iw} := \begin{cases} 1 & \text{for } r_i - d_{iW} \geq 0 \\ 0 & \text{otherwise} \end{cases} \tag{3.3}$$

where the distance from agent i to obstacle W is

$$d_{iW} := \inf_{\mathbf{x} \in \mathcal{W}_W} ||\mathbf{p}_i - \mathbf{x}||. \tag{3.4}$$

The violation caused by an obstacle is determined by

$$g_{iW} := \max\left(0, r_i - d_{iW}\right). \tag{3.5}$$

3.2 Social-ACC

The social force model of Helbing only considers circular comfort zones. This means that the desired distance between agents is equal in every direction. Since an agent cannot change its direction directly (due to the nonholonomic constraint), the lateral distance between agents may be smaller than the longitudinal distance. This difference in distance can only be achieved by taking care of the road's geometry. After the inclusion of geometry, the size of the comfort zone is made speed dependent such that the minimum amount of road is used by each agent without decreasing safety.

3.2.1 Inter-agent interactions

To include geometry without changing the current measure of violation (3.2) and (3.5), different possibilities to change the interaction function are discussed.

The first possibility is to change the indicator function I_{ij} such that it contains geometry (see Figure 3.4a). While changing the indicator function, the violation (still based on the radius, Figure 3.3b) is determined by the largest dimension of the geometric comfort zone. Thus, the possibility exists that

$$\exists \mathbf{q}_{ij} \in \left\{ \mathcal{Q}_{ij} \mid \left(I_{ij}(\mathbf{q}_{ij}) = 0 \wedge g_{ij}(\mathbf{q}_{ij}) > 0 \right) \right\}.$$

Therefore the possibility exists that there is a jump in the applied force (see Figure 3.4b). This jump will cause discomfort for passengers and will increase the stiffness of the multi-agent system significantly. Both effects are undesirable.

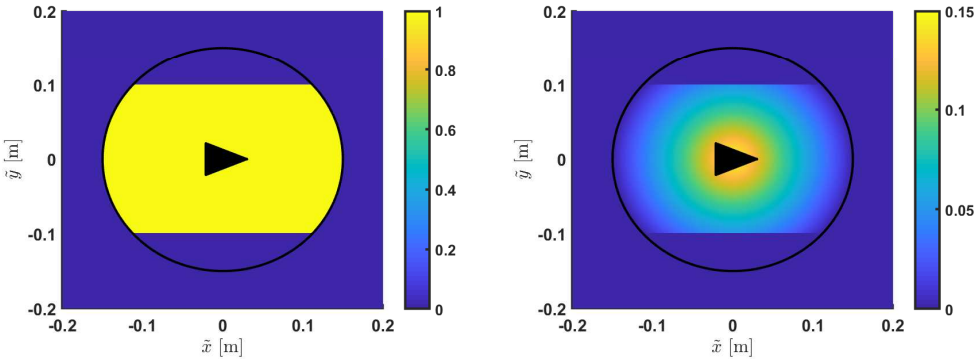

(a) $\Upsilon_{ij} := I_{ij}$ (b) $\Upsilon_{ij} g_{ij}$

Figure 3.4: Visualization of (a) indicator function defined by the geometric indicator function and (b) the product of the interaction and violation function.

A different possibility to add geometry without increasing the stiffness is to smooth the indicator function by taking the convolution with a Gaussian function $\Upsilon_{ij} := I_{ij} * G$ However, the Gaussian function G has an asymptote at 0 and therefore the convolution also has an asymptote at 0. The interaction function with an asymptote at 0 can be interpreted as an always exciting interaction between agents. Since it is in appropriate to assume that all agents always interact, a different method is required.

Replacing the Gaussian function for a bump function $\Upsilon_{ij} := I_{ij} * \tilde{\Psi}_i$, the asymptote is avoided. According to [49], the support of the convolution of $f : \mathbb{R}^N \to \mathbb{R}$ and $g : \mathbb{R}^N \to \mathbb{R}$

$$\operatorname{supp}(f * g) \subset \overline{\operatorname{supp}(f) + \operatorname{supp}(g)},$$

where $\overline{\ }$ denotes the continuous extension and support is defined as:

Definition 6. *The support of the real-valued function f is the subset of the domain $\mathcal{X}$ containing those elements which are not mapped to zero*

$$\operatorname{supp}(f) := \{x \in \mathcal{X} | f(x) \neq 0\}.$$

Hence, by taking the convolution of the indicator and a bump function $\tilde{\Psi}_i$, the interaction function can have support outside the support of the indicator function. This means that there can be interaction before the comfort zones overlap, which is also inappropriate. Therefore, it is desirable to have

$$\operatorname{supp}(\Upsilon_{ij}) \subset \operatorname{supp}(I_{ij})$$

such that there is no interaction before the (circular) comfort zones overlap.

A possibility to guarantee this is by setting the interaction function as product of the indicator and bump function $\Upsilon_{ij} := I_{ij} \tilde{\Psi}_i$, resulting in

$$\operatorname{supp}(\Upsilon_{ij}) := \operatorname{supp}(I_{ij}) \cap \operatorname{supp}\left(\tilde{\Psi}_i\right).$$

The only disadvantage of this method is that the interaction function is not guaranteed to be smooth.

A complete overview of the discussed possibilities and their implications is given in Table 3.1. Eventually the product method is chosen, since it can guarantee no interaction before the circular comfort zones are violated. Furthermore, this method guarantees a gradually increasing force since $\operatorname{supp}(I_{ij}) = \operatorname{supp}(g_{ij})$ and g_{ij} is a gradually increasing function.

Table 3.1: The implications of the different methods to add geometry.

Method	reduces stiffness	no asymptote	smooths only inwards	smoothing guaranteed
Geometric indicator function	✗	✓	✗	✗
Convolution of Gaussian function and indicator function	✓	✗	✗	✓
Convolution of bump function and indicator function	✓	✓	✗	✓
Product of bump function and indicator function	✓	✓	✓	✗

Choosing the product methods also allows smoothing of the indicator functions (3.1) and (3.3) only in the lateral direction (of the agent). Here the advantage is that the comfort zone is still very similar to the circular one, while taking care of the road geometry. To do so, the bump function of agent i is created by the product of two 1D-bump functions

$$\tilde{\Psi}_i(\tilde{\mathbf{z}}_i) := \psi_{i,\tilde{x}}(\tilde{x}_i)\psi_{i,\tilde{y}}(\tilde{y}_i)$$

in the longitudinal and lateral direction of the agent respectively. Here $\tilde{\mathbf{z}}_i := \tilde{x}_i\mathbf{e}_1^i + \tilde{y}_i\mathbf{e}_2^i = \begin{pmatrix}\tilde{x}_i & \tilde{y}_i\end{pmatrix}\mathbf{e}^i$, is a vector expressed in the agent's local frame. The 1D-bump function $\psi : \mathbb{R} \to [0,1]$ is defined in Appendix A. To create the desired geometry, the lateral 1D bump function $\psi_{i,\tilde{y}}(\tilde{y}_i)$ has to fulfill the following constraints

$$\begin{cases} 0 & \text{for} \quad \tilde{y}_i \leq -\frac{w_{c,i}}{2} \text{ and } \tilde{y}_i \geq \frac{w_{c,i}}{2} \\ 1 & \text{for} \quad -\xi_{w,i}\frac{w_{c,i}}{2} \leq \tilde{y}_i \leq \xi_{w,i}\frac{w_{c,i}}{2} \end{cases}.$$

Here the (geometric) comfort zone width is chosen equal to the lane width $w_{c,i} = w_\ell$ and the lateral smoothing factor $0 \leq \xi_{w,i} < 1$ determines the amount of smoothing. For $\xi_{w,i} = 0$ the function is completely smooth.

To only smooth the indicator function in the lateral direction, the longitudinal bump function has to fulfill the following constraints

$$1 \quad \text{for} \quad -r_i \leq \tilde{x}_i \leq r_i.$$

The result is shown in Figure 3.5, where it can be seen that the indicator function is only smoothed in the lateral direction and does not contain jumps.

By using the 2D-bump function $\tilde{\Psi}_i : \mathbb{R}^2 \to \mathbb{R}$, the next challenge is to find an appropriate input for this function. The input is a point in $\mathbb{R}^2$ which should represent the violation of the geometric comfort zone based on the overlap of the original circular comfort zones. If this point falls outside $\operatorname{supp}(\Psi_i)$, the geometric comfort zone should not be violated. If the geometric comfort zone is violated, the point should fall inside $\operatorname{supp}(\Psi_i)$.

To provide such an input, the local violation vector is defined

$$\tilde{\mathbf{g}}_{ij} := \left(r_i - \frac{r_i}{r_i + r_j} g_{ij}\right) \tilde{\mathbf{n}}_{ij}.$$

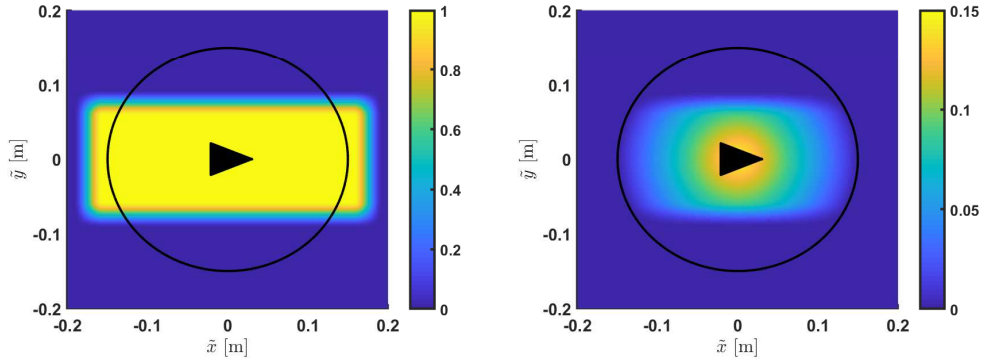

(a) Ψ_i (b) Υg_{ij}

Figure 3.5: Visualization of (a) the bump function Ψ_i and (b) the product of the interaction function $\Upsilon := I_{ij}\Psi_i$ and violation function g_{ij}.

Here $\tilde{\mathbf{n}}_{ij}$ is the normal vector pointing from agent j to i expressed in the agent frame since $\tilde{\Psi}_i$ is also defined in the agent frame. For equally sized comfort zones, the local violation vector represents the midpoint of the comfort zone overlap. If the comfort zones are not equally sized, the midpoint is changed proportional to the comfort zone ratio of the two agents. A visualization is given in Figure 3.6.

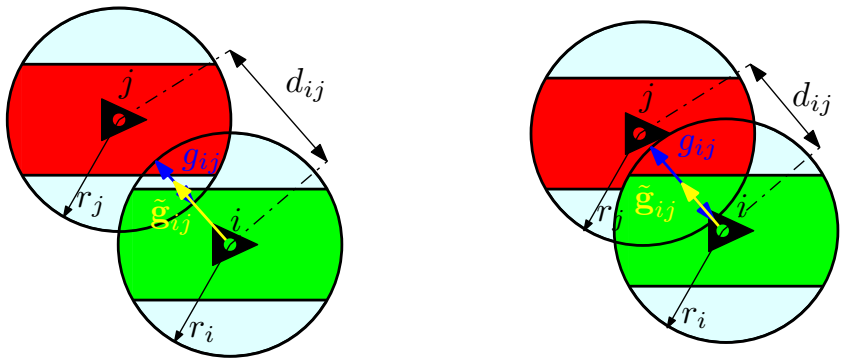

(a) (b)

Figure 3.6: Visualization of the local violation vector $\tilde{\mathbf{g}}_{ij}$ and its working in combination with the 2D-bump function. The local violation vector (a) is outside the support of the 2D-bump function if the two geometric comfort zones do not overlap and (b) inside if they do overlap.

Altogether, the smoothing function Ψ_{ij} becomes

$$\Psi_{ij} := \tilde{\Psi}_{ij}(\tilde{\mathbf{g}}_{ij}) = \psi_{i,\tilde{x}}(\tilde{g}_{ij,x})\psi_{i,\tilde{y}}(\tilde{g}_{ij,y}) \tag{3.6}$$

and thus the interaction function of social-ACC is defined as

$$\Upsilon_{ij} := I_{ij}\Psi_{ij},$$

where I_{ij} as defined in (3.1) and Ψ_{ij} as defined in (3.6).

Remark. *Without any difference in the agent orientation, the interaction function works as desired. However, if there is a large difference between the agents' orientations, an agent can experience violation while the geometric comfort zone is not violated (see Figure 3.7). Since all agents drive in the same direction and the lane change only requires a relatively small change in orientation, the effect of this flaw should be limited. Furthermore, the ratio between the geometric comfort zone dimensions and the radius is kept relatively large to limit the effect of this flaw.*

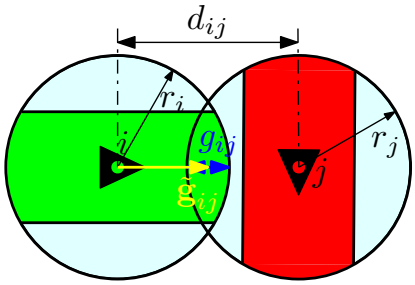

Figure 3.7: Agent i is experiencing violation while the geometric comfort zones do not overlap.

With the currently defined interaction rules, the effect of violation at the front and at the back of the comfort zone is equal. However, it is more likely to react heavier on a braking agent a head than a tailgater. The smoothing function can be used to smooth the indicator function such that the effect of tailgaters is reduced (see Figure 3.8). To smooth the back of the comfort zone, the longitudinal bump function $\psi_{i,\tilde{x}}(\tilde{x}_i)$ should fulfill the following constraints

$$\begin{cases} 0 & \text{for} \quad \tilde{x}_i \leq -\ell_{b,i} \text{ and } \tilde{x}_i > r_i \\ 1 & \text{for} \quad -\xi_{b,i} r_i \leq \tilde{x}_i \leq r_i \end{cases}$$

where $0 \leq \xi_{b,i} \leq 1$ is the back smoothing factor and $\ell_{b,i}$ describes the length of the comfort zone in the back. If $\xi_{b,i} = 1$ then $\ell_{b,i} > r_i$ due to the definition of the bump function.

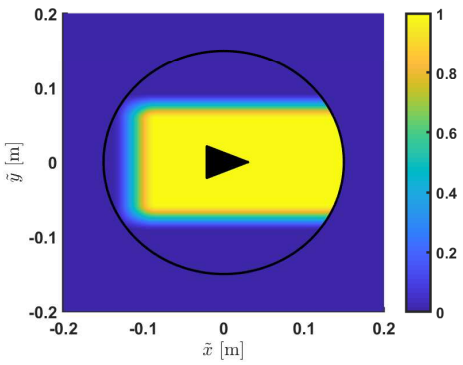

Figure 3.8: The indicator function combined with the smoothing function to reduce the effect of tailgaters.

The currently created geometry of the comfort zone does not have a shape that in particular induces merging behavior. To do so, additional geometry rules are added to the current comfort zones. Three different possibilities are proposed.

The first possibility to induce merging behavior is by adding a point to the front of the comfort zone (see Figure 3.9a). With this point the agent should be able to squeeze itself between the other agents. The second possibility is adding a point to the back of the comfort zone instead of the front (see Figure 3.9b). With this shape the agent should react less on tailgaters, being more egoistic, pushing itself between the other agents. The last possibility is a combination of both options, where a point is added to the front and the back (see Figure 3.9c). The additional geometry rules are applied by making the lateral smoothing factor $\xi_{w,i}(\tilde{x}_i)$ depend on the local longitudinal coordinates.

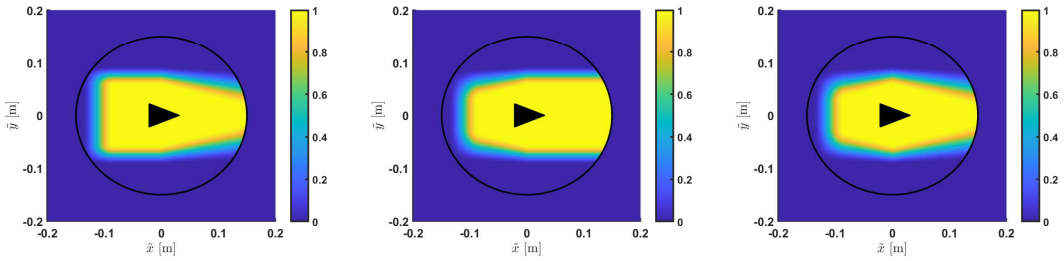

(a) (b) (c)

Figure 3.9: Three possible geometric comfort zones which induce merging behavior. (a) with a point at the front, (b) with a point at the back and (c) a combination with a point at the front and back.

3.2.2 Environmental interactions

Similarly to the inter-agent interactions, geometry is applied to the environmental interactions.

$$\Upsilon_{iw} := I_{iW}\Psi_{iW} = I_{iw}\tilde{\Psi}_i(\mathbf{g}_{iW})$$

However, using the violation based on the distance from agent i to obstacle d_{iW} is not appropriate anymore. The point used to determine the distance as in (3.4) may be outside the geometric comfort zone, while another point of the obstacle may be inside the geometric comfort zone (see Figure 3.10). Therefore, the violation is based on the point $\hat{\mathbf{x}}$ in the obstacle set $\mathcal{W}_W$, causing the most effective violation

$$\hat{\mathbf{x}} := \arg\max_{\mathbf{x}\in\mathcal{W}_W} \left(\Upsilon_{iW}(\mathbf{p}_i, \mathbf{v}_i, \mathbf{x}) \max\left(0, r_i - ||\mathbf{x} - \mathbf{p}_i||\right)\right).$$

The distance used to determine the violation is then

$$\hat{d}_{iW} := ||\hat{\mathbf{x}} - \mathbf{p}_i||,$$

where the violation is defined as

$$g_{iW} := \max\left(0, r_i - \hat{d}_{iW}\right). \tag{3.7}$$

The environmental interaction force is determined by the interaction rule described in (2.4). Here the normal vector $\mathbf{n}_{iW}$ is pointing from $\hat{\mathbf{x}}$ to agent i and tangential vector $\mathbf{t}_{iW}$ is determined accordingly based on a righthanded system.

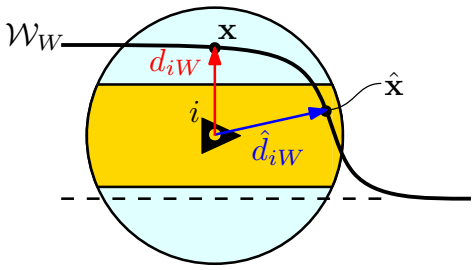

Figure 3.10: The point $\mathbf{x}$ used to determine the distance from agent$i$ to the obstacle W falls inside the circular comfort zone (cyan) but outside the geometric comfort zone (orange). Therefore, the new distance $\hat{d}_{iW}$ based on $\hat{\mathbf{x}}$ is defined.

A disadvantage of geometric comfort zones is that the rotation of the agent can increase the violation. Initially the agent's geometric comfort zone is not violated since the most effective distance $\hat{d}_{iW}$ is outside the geometric comfort zone, see Figure 3.11a. When turning away from the boundary suddenly there is a huge violation since the most effective distance $\hat{d}_{iW}$ is now inside the geometric comfort zone, see Figure 3.11b. This violation causes the agent to thrust forward, which is undesired. Therefore, the geometric comfort zone of an agent for obstacles only exists in the forward direction, indicated by the dark orange area in Figure 3.11. This reduction of the obstacle comfort zone will not cause problems since the agents cannot drive backwards ($v_i \geq 0$).

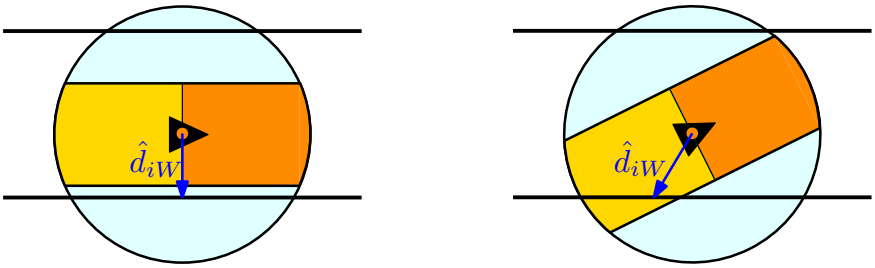

(a) (b)

Figure 3.11: (a) Initially the geometric comfort zone (orange) is not violated. (b) After rotation the geometric comfort zone is violated. By only applying a geometric comfort zone to the front (dark orange) the effect is removed.

3.2.3 Spacing policy

The next step is to make the comfort zone speed dependent such that only the minimum amount of road is used without reducing safety. Over the years, different spacing policies are developed [50–52]. The three spacing policies often found in literature are the constant spacing policy, the constant time spacing policy and the nonlinear spacing policy. The constant time spacing policy is often used since the constant spacing policy is known to cause string unstable behavior. Furthermore, the nonlinear spacing policies are not crystallized yet since they are currently ongoing research. It is known that the constant time spacing policies can increase the string stability [7]. However, in [53] it is shown that two-sided interaction (Bi-ACC) may negatively influence the string stability. Despite that, the constant time spacing policy is adopted, since the implementations of [7, 53] use attractive and repulsive forces, while the social force model only uses repulsive forces thus similar effect is not guaranteed.

By adopting the constant time spacing policy, the comfort zone radius of agent i is

$$r_i := r_{i,0} + h_i ||\mathbf{v}_i||$$

with standstill distance $r_{i,0}$ and headway-time h_i.

The addition of this linear spacing policy results in a growth problem if $\gamma_i = 0$, as in the original social force model (2.2). Assume that two agents are driving with the same (initial) speed and their comfort zone is violated (Figure 3.12a), both agents experience the same force. Agent i will accelerate and agent j will decelerate. Therefore, the comfort zone of agent i will grow and the comfort zone of agent j will decrease. However, the violation grows or remains the same if h_i is sufficiently large (Figure 3.12b). Neither the speed nor the comfort zone size is bounded, causing the velocity state to increase instantly.

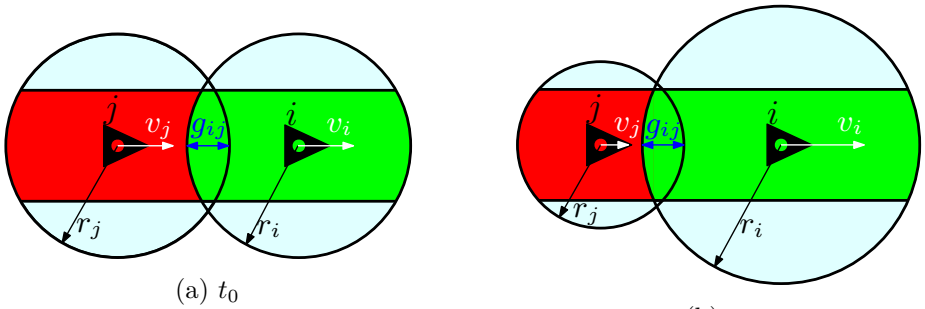

(a) t_0 (b) t_1

Figure 3.12: Initially two agents are driving with the same speed and (a) there is comfort zone violation g_{ij}. Due to the violation the agents will react accordingly. Agent j will decelerate while agent i accelerate. Due the spacing policy (b) the amount of violation is not (necessarily) reduced.

The quadratic speed regulation term γ_i is introduced such that the comfort zone is bounded in a "natural" way, instead of adding a limitation. The quadratic speed regulation term will eventually be the "winning term" and stop the vehicle to accelerate and the comfort zone to grow. This is shown in Appendix C where the 2D scenario is simplified to a 1D case.

Adding the spacing policy also results in two agents experiencing the same violation, while their comfort zones do not have the same size. In general, a fast driving agent will have a large comfort zone with respect to a slower agent. With the current interaction rule, both agent experience the same violation. However, it is intuitive to let the fast driving agent undertake a larger control action, thus should experiencing more violation. To do so, the violation is scaled by using the comfort zone ratio between the two agents

$$g_{ij} := \frac{r_i}{r_i + r_j} \max\left(0, r_{ij} - d_{ij}\right).$$

By redefining the violation function, the local violation vector should also be redefined accordingly

$$\tilde{\mathbf{g}}_{ij} := \left(r_i - g_{ij}\right) \tilde{\mathbf{n}}_{ij}.$$

3.3 2D-ACC

The special thing of the earlier derived social-ACC is that both agents will experience a force if their comfort zone is violated. The mutual experience of violation is due to the overlapping comfort zones as measure of violation. The working principle of ACC is based on a single sided measure of violation such that only the agent whose comfort zone is violated experiences a force. In general, ACC uses the difference between the desired inter-agent distance and the agent's position as measure of violation. Furthermore, ACC is merely focused on interactions at the front and does not take tailgaters into account. To create a comparison between the earlier derived social-ACC and a 2D variant of ACC, 2D-ACC is derived in the social force framework.

To create the single-sided measure of violation, the other agent's position inside the comfort zone is used. Thus, the comfort zone of agent i is violated if agent j is in it

$$I_{ij} := \begin{cases} 1 & \text{for } 2 \cdot r_i - d_{ij} \geq 0 \\ 0 & \text{otherwise} \end{cases},$$

where d_{ij} is the distance between two agents. To maintain the same spacing as with social-ACC, the agent's comfort zone is doubled. The violation

$$g_{ij} := \frac{1}{2}\max(0, 2 \cdot r_i - d_{ij}), \tag{3.8}$$

is based on the other agent's position in the comfort zone. The factor $\frac{1}{2}$ is added to create the same weighting as with social-ACC, which represents the comfort zone ratio scaling.

This 2D-ACC can be seen as a special case of social-ACC where the other agent's comfort zone is neglected by setting $r_j = 0$. The total interaction function is described by

$$\Upsilon_{ij} := I_{ij}\Psi_{ij} = I_{ij}\tilde{\Psi}_i\left(\mathbf{g}_{ij}\right)$$

where $\mathbf{g}_{ij}$ is based on (3.8).

For a real ACC working principle, the back of the comfort zone should be removed, since ACC does not take tailgaters into account. To approach a more novel ACC method, e.g. bidirectional-ACC as in the work of Nieuwenhuijze [53], the back of the comfort zone could be maintained. If the effect of tailgaters is not reduced, the spacing policy still requires the quadratic speed regulation term $\gamma_i > 0$. Furthermore, the environmental interactions are as defined in social-ACC.

Remark. *This implementation of ACC differs from ACC used in the platooning context as in [6, 7, 36, 53] where a vehicle is attracted to the proceeding vehicle such that the gap is closed. This implementation only uses repulsive forces for collision avoidance, which is comparable with the currently implemented ACC in today's vehicles [54–56].*

3.4 Summary of the interaction designs

The original interactions of the social force model by Helbing are based on circular comfort zones. The agents interact if their comfort zones overlap. The experienced interaction force is proportional to the comfort zone overlap (violation).

In social-ACC the comfort zone radius is made speed dependent by applying the constant time spacing policy. Adding the spacing policy requires compensation by γ_i to limit the growth effect. Since it is desired to have a larger longitudinal inter-agent distance than lateral inter-agent distance, the road geometry is taken into account. This is done by setting the interaction term $\Upsilon_{ij} \in [0, 1]$ as the product of the smoothing function $\Psi_{ij} \in [0, 1]$ and the indicator function $I_{ij} \in \{0, 1\}$. Here the indicator and violation functions are the same as in the work of Rodriguez-Angeles et al. [22]. However, the environmental violation function giW is based on the most effective point of violation and the comfort zone at the back of the agent is neglected.

In 2D-ACC, the working principle of ACC is embedded into the social force framework as a special case of social-ACC. The comfort zone of the other agent is neglected and the agent its comfort zone is enlarged by a factor two to keep an equal weighting.

An overview of the different features per developed method is given in Table 3.2.

Table 3.2: Overview of the developed methods and their features.

Method	Social	Geometry	Spacing Policy
Helbing	✓	✗	✗
Social-ACC	✓	✓	✓
2D-ACC	✗	✓	✓

Chapter 4

Simulation results

The complete model is derived in the previous chapters. This chapter will first cover the simulation environment, the executed simulations and the default settings for the highlighted simulations.

Thereafter, the effect of the design choices is shown, starting with the addition of the nonholonomic constraint by replacing the mass point with the unicycle kinematics. This is followed by the effect of the spacing policy and a comparison of social-ACC with 2D-ACC. Furthermore, the effect of the comfort zone at the back is investigated since this is one of the two main differences between social-ACC and 2D-ACC. Since it is inappropriate to assume that agents can increase their speed without limit (e.g. due to speed limits on the highway), the effect of a speed saturation is also investigated. Next to that, the effect of geometry on the collective behavior is analyzed. Finally, all results are summarized and a complete overview is given.

4.1 Simulation environment

The complete model as described in Chapters 2 and 3 is implemented in the MATLAB Simulink environment using (level 2) S-functions. Three different S-functions are developed: one describing the social force model; the second, the projection method to link the social force model to the unicycle kinematics; and the last, one the unicycle kinematics.

In Simulink the differential equations are solved by the built-in `ode45` solver, using the Dormand-Prince method, a member of the Runge-Kutta family of ordinary differential equation (ODE) solvers. This solver is typically used to solve non-stiff differential equations, which is applicable in this case since the stiffness of the problem is reduced using the product of the indicator and smoothing function. The settings of the ODE solver are in Table 4.1.

Many simulations have been executed to characterize the working of the different interaction rules. In Table 4.2 the used set of values for each parameter is shown per interaction method. Simulations for all possible parameter combinations are executed and analyzed for each interaction method. This chapters only highlights specific simulations, characterizing the outcome of other similar simulations.

Table 4.1: MATLAB Simulink ODE solver settings.

Variable	**Setting**
Solver	`ode45`
Relative error tolerance	$1 \cdot 10^{-4}$
Absolute error tolerance	$1 \cdot 10^{-6}$
Upper bound on the step size	1

Table 4.2: The varied parameters and corresponding value set. Simulations for all possible parameter combinations are executed and analyzed for each interaction method.

	Original Helbing (mass point)	**Helbing (unicycle)**	**Social-ACC**	**2D-ACC**
n	$\{2, 4, 8, 20\}$	$\{2, 4, 8\}$	$\{2, 4, 8, 20\}$	$\{2, 4, 8, 20\}$
h_i	0	0	$\{0, 0.5, 1\}$	$\{0, 1\}$
$v_i^{\max}$	∞	∞	$\{v_i^c, 1.1v_i^c, 1.2v_i^c, 1.5v_i^c, \infty\}$	$\{v_i^c, \infty\}$
$\xi_{w,i}$	–	–	$\{0.25, 0.50, 0.75, 0.90\}$	$\{0.50, 0.75\}$
$\xi_{b,i}$	–	–	$\{0, 0.25, 0.50, 0.75, 1\}$	0

The parameter settings of the social force model which are used for all simulations (in this report), unless indicated otherwise, are shown in Table 4.3. These values are equal to the used values for the bottleneck scenery in the work of Rodriguez-Angeles et al. [22], except for the newly introduced parameters. All values are based on the e-puck mobile robot, which give the advantage that it can be tested at a later stage.

Table 4.3: Standard used parameter values unless indicated otherwise.

Parameter	h_i	$r_{i,0}$	$w_{c,i}$	$\xi_{w,i}$	$\ell_{b,i}$	$\xi_{b,i}$	v_i^c	$v_i^{\max}$	γ_i	k_i	κ_i	τ_i	m_i
Value	1	0.1	0.2	0.5	$2r_i$	1	0.05	∞	5	4	2	0.5	0.2

All initial conditions are chosen such that each agent starts and stays interaction-free until the first agent experiences an interaction force due to the road narrowing. The used initial conditions are in Table 4.4.

Table 4.4: The initial conditions of each agent i, with agent set $\mathcal{V}$ and natural number set $\mathbb{N}$. Thus, the lower lane agents are denoted with an odd number, while the upper lane agents are denoted with an even number.

State	$x_i(0)$	$y_i(0)$	$\theta_i(0)$	$v_i(0)$
Lower lane agent $i \in \{\mathcal{V} \cap 2\mathbb{N}+1\}$	$-5-(i-1)r_i$	$-\frac{1}{2}w_\ell$	0	v_i^c
Upper lane agent $i \in \{\mathcal{V} \cap 2\mathbb{N}\}$	$-5-(i-2)r_i$	$\frac{1}{2}w_\ell$	0	v_i^c

A simulation is terminated if all agents have passed the line $x = 5$ and the stress of all agents is $\sigma_i \leq 0.05$. The stress requirement is added so that the simulation stops if there is almost no interaction, thus the agents are again driving in a steady state. After terminating the simulation, the output is saved to a `.mat` file, which is used for post-processing. The saved data signals in the output file are in Table 4.5, furthermore the `.mat` file contains all parameter settings.

All measurements and figures in this chapter are made by post-processing the signals from Table 4.5. Frequently used measures are the flow time and cycle time factor (CTF), see Definitions 1 and 2 respectively. In this chapter, the measurements are based on the interval $x = -5$ to $x = 5$, thus $\Delta x = 10$. According to Definition 2, the derived nominal flow time is $\bar{\varphi} = 200$. Hence, the difference between the CTF and the flow time is a factor 200, unless a different interval or cruise speed is used.

Furthermore, the animations and snapshots from the simulations are also made by post-processing. In the animations and snapshots (e.g. Figure 4.1) the agent (considered as an e-puck mobile robot) is represented by a black circle with a triangle in it. The triangle inside the black circle indicates the orientation of the agent. The comfort zone of an agent is represented by the colored shape (circle or rectangle) around the black circle. To distinguish upper and lower lane agents after merging, the comfort zones are marked

Table 4.5: Simulation output signals

Symbol	Description
t	time steps
$x(t)$	x-positions
$y(t)$	y-positions
$\theta(t)$	orientation
$v(t)$	forward speed
$\omega(t)$	rotation speed
$a_x^d(t)$	desired acceleration in x direction
$a_y^d(t)$	desired acceleration in y direction
$\sigma(t)$	stress

with different colors. Comfort zones of upper lane agents are marked light blue, while the comfort zones of lower lane agents are marked light purple. For circular comfort zones the visualization of the comfort zone is a circle (e.g. in Figure 4.1), while for geometric comfort zones the visualization is simplified to a rectangle (e.g. in Figure 4.5).

The outer dimensions of the simplified comfort zone represent the closure of supp (Ψ_{ij}). The additional geometry is thus not (fully) visible in the animations and snapshots. The red arrows in the animations and snapshot represent the agent's velocity, which is scaled with a factor 3 for a better visibility.

4.2 The addition of the nonholonomic constraint

The original social force model of Helbing et al. [21] uses point masses, as most models with artificial potential fields do. However, from [16] it is known that agents with similar interaction rules, but different dynamics can show different collective behavior. Therefore, the point mass is replaced by the unicycle kinematics as elaborated in Sections 2.1.2 and 2.1.3. Rewriting the nonholonomic constraint to determine inputs of the unicycle model as in the work of Rodriguez-Angeles et al. [22], can results in unstable behavior.

Rewriting the nonholonomic constraint results in the following control strategy (see Appendix B for derivation). The rotation speed of agent i is set to

$$\omega_i := \frac{a_{i,y}^d v_{i,x}^d - a_{i,x}^d v_{i,y}^d}{\epsilon + ||\mathbf{v}_i^d||^2}, \tag{4.1}$$

where $\mathbf{v}_i^d := \begin{pmatrix} v_{i,x}^d & v_{i,y}^d \end{pmatrix}$ is the desired velocity obtained by integrating the output of the social force model (the desired acceleration $\mathbf{a}_i^d$). Here $0 < \epsilon \ll 1$ is added to avoid singularities when $v_i = 0$. The forward speed is set to

$$v_i := ||\mathbf{v}_i^d||.$$

The unstable behavior is caused by setting the agent's forward velocity equal to the magnitude of the desired velocity without taking the agent's orientation into account. Assume that the agent's comfort zone is violated, creating a force perpendicular to the agent's orientation. The desired velocity changes accordingly, thus points in the same direction. The speed of the agent is set to the amplitude of this desired velocity, while his orientation still has to change according to (4.1). Therefore, the agent starts driving in the wrong direction, causing more violation increasing the interaction force, causing the agent to drive even further in the wrong direction. Hence, this effect reinforces itself, resulting in the unstable behavior.

This effect is shown using a simulation with $n = 2$, $h_i = 0$, $v_i^c = 0.01$ and $\epsilon_i = 0.01$. The animation of this simulation can be found at https://youtu.be/RYpGI7wcK00[1] and the corresponding snapshots are shown in Figure 4.1. It can be seen that velocity (red arrow) has the same amplitude as the desired velocity (blue arrow), although it is pointing in the wrong direction. This results in the agent driving faster into the boundary instead of driving away.

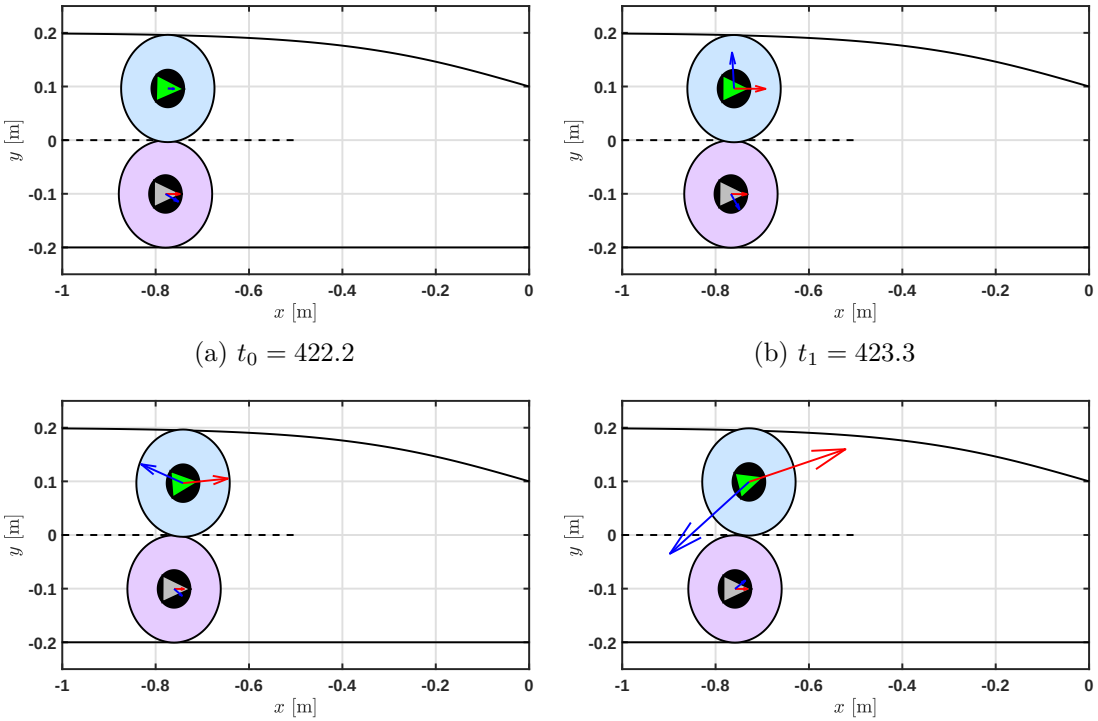

(a) $t_0 = 422.2$ (b) $t_1 = 423.3$

(c) $t_2 = 423.9$ (d) $t_3 = 424.2$

Figure 4.1: Four snapshots from a simulation with unicycle kinematics and the rewritten nonholonomic constraint to obtain the velocity inputs from the social force model. The red arrow presents the agent velocity, while the blue arrow represents the desired velocity. Setting the forward velocity to the magnitude of the desired velocity, without taking the orientation into account, results in the agent driving in the wrong direction increasing the desired control action created by the social force model. The used settings are $h_i = 0$, $v_i^c = 0.01$ and $\epsilon_i = 0.01$.

This unstable behavior emphasize the importance of taking the constraints into account when modeling. In the newly developed model, the constraints are taken into account by embedding them into the dynamics. The projection from the desired acceleration on the unicycle orientation is taken to determine the forward and rotation speed. This does not cause unwanted behavior, which is shown using a simulation for a system with $n = 8$ and $h_i = 0$. The animation of this simulation can be found at https://youtu.be/XuxFNpQUxG0[2] and the corresponding snapshots are shown in Figure 4.2. Here it can be seen that the agents are merging fluently without showing unstable behavior.

[1] on the provided USB-stick listed as: `01_Unicycle_kinematics_linked_by_rewriting_the_nonholonomic_constraint.avi`.

[2] on the provided USB-stick listed as: `02_Unicycle_kinematics_with_projection_method.avi`.

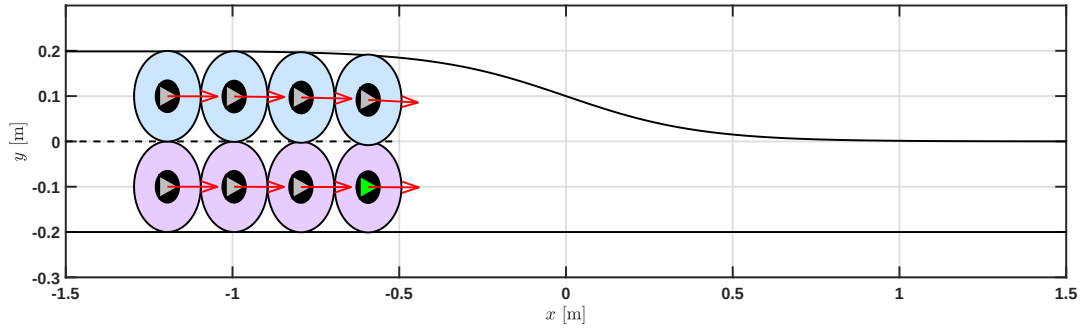

(a) $t_0 = 88.1$

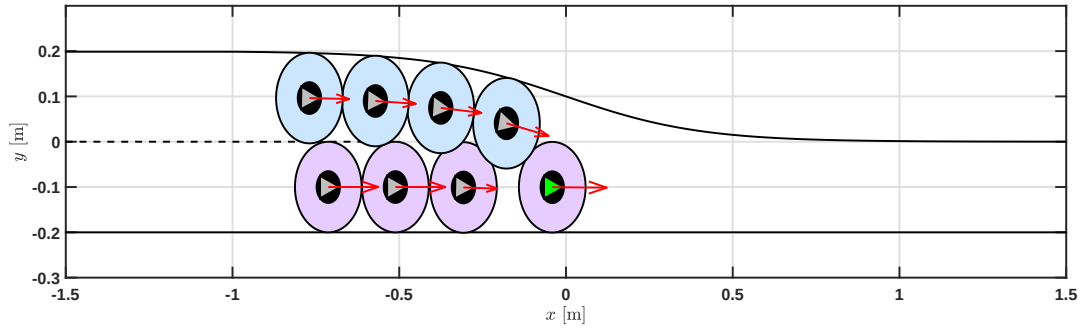

(b) $t_1 = 97.7$

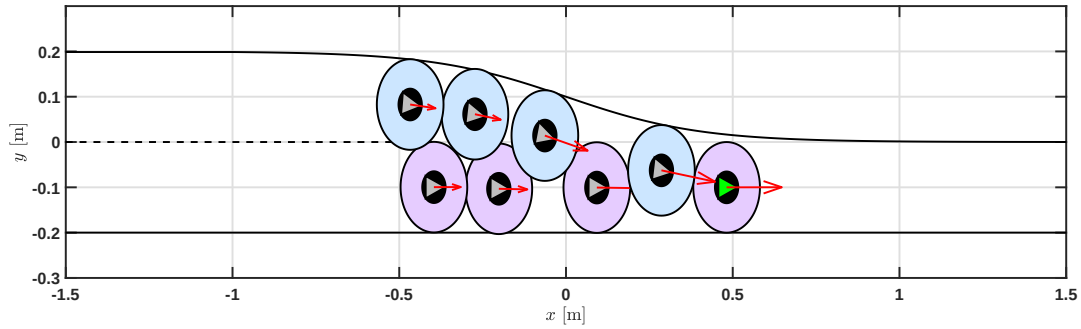

(c) $t_2 = 106.9$

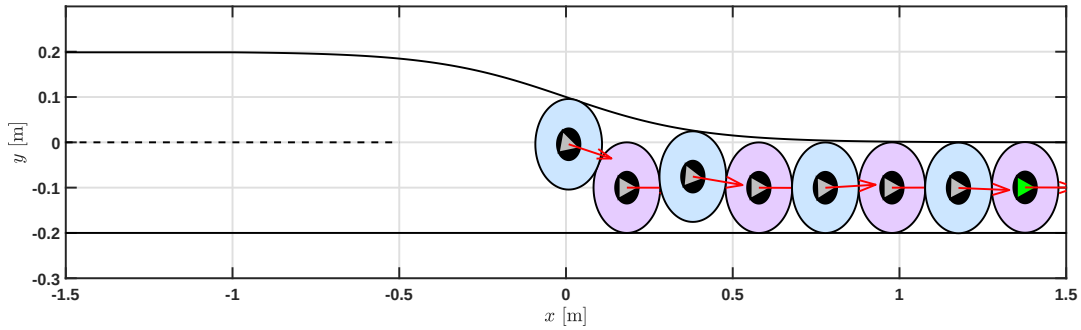

(d) $t_3 = 124.0$

Figure 4.2: Snapshots from a simulation with the projection method, unicycle kinematics and $h_i = 0$. The upper lane agents are forced to the lower lane by the boundary. Due to the overlapping comfort zones, the lower lane agents are forced to create gaps to let the upper lane agents merge. Therefore the agents at the front increase their speed (red arrow) and drive faster than their (desired) cruise speed / initial speed.

The animation and the corresponding snapshots also show the working principle of the social force model. Initially the agents are driving to the road narrowing, without any gaps between their comfort zones. At the road narrowing the upper lane agents are forced to move downwards by the road boundary. Causing the upper and lower lane agents' comfort zones to overlap, resulting in interaction. Due to this interaction, the upper lane agents are pushing the lower lane agents away such that gaps arise and they can merge.

To show the effect of the pushing-behavior, the flow time and CTF are measured for a system with $n = 20$ and $h_i = 0$. The results are shown in Table 4.6. Due to the pushing, the average CTF is close to 1. Meaning that the average flow time is close to the nominal flow time.

Table 4.6: The average flow time and CTF of 20 agents with unicycle kinematics, without geometry and $h_i = 0$.

Model:	**Unicycle**
Average flow time	203.020
Average CTF	1.0151

Due to the pushing, the first agents are required to drive faster than their desired speed, while the last agents are required to drive slower (see Figure 4.3). Hence, the agents share discomfort by not driving on their desired speed, but improving the collective performance.

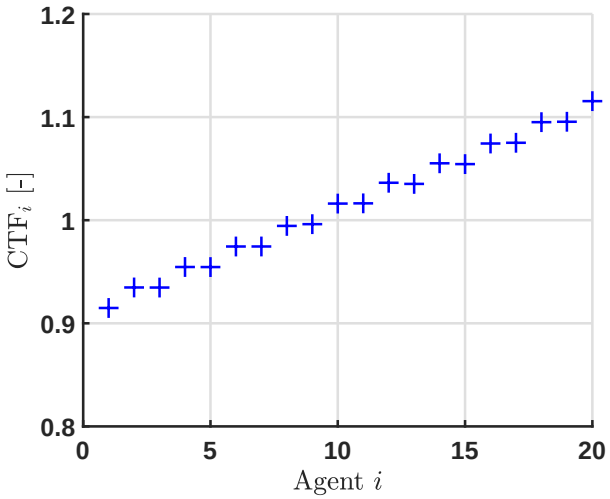

Figure 4.3: The CTF distribution for 20 agents with unicycle kinematics, without geometry and $h_i = 0$. A CTF value lower than 1 implies that the flow time is lower than the nominal flow time.

4.3 The effect of the spacing policy

Applying the spacing policy as elaborated in Section 3.2.3 should result in agents only using the required amount of road, thereby improving the flow through the road narrowing. By means of simulations, the effect of the spacing policy and the applied geometry is characterized as following:

i) using larger headway times results in a decrease of the CTF;

ii) using larger headway times results in a decrease of road usage during queuing;

To show these two effects, three different cases are used. Three cases are derived as following: The minimally used comfort zone radius r_i should larger or equal to the lane width since it is undesirable that agents can drive parallel in the same lane. To show the effect of h_i, the stand still distance of each case is chosen such that the comfort zone radius is equal in all simulations when driving at the desired cruise speed

$$r_{i,0} + h_i v_i^c = 0.15.$$

To not influence agents on the adjunct lane until the road narrows, the lateral geometry is applied as shown in Figure 3.5 and elaborated in Section 3.2.1. The application of the lateral geometry holds for all further simulations in this chapter unless indicated otherwise. One may also recall that for the environmental interactions the comfort zone at the back is removed as explained in Section 3.2.2.

The effect of the different cases on the flow time and CTF is shown in Table 4.7. It can be seen that a larger headway time decreases the average flow time. Using the CTF distributions in Figure 4.4 it can be verified that the working principle has not changed since the first agents still have a $CTF < 1$. Hence, statement (i) is shown. However, an additional statement has to be made accordingly:

iii) using larger comfort zones with geometry decreases the CTF (with respect to the circular comfort zones used in the previous section).

In Figure 4.4 it is shown that even without the application of the spacing policy ($h_i = 0$), the CTF is significantly higher than in the previous section, where no geometry is applied.

Table 4.7: The average flow time and CTF of 20 agents with different spacing policy settings.

Setting:	h_i	0.0	0.5	1.0
	$r_{i,0}$	0.15	0.125	0.1
Average flow time		220.147	217.233	215.107
Average CTF		1.1007	1.0862	1.0755

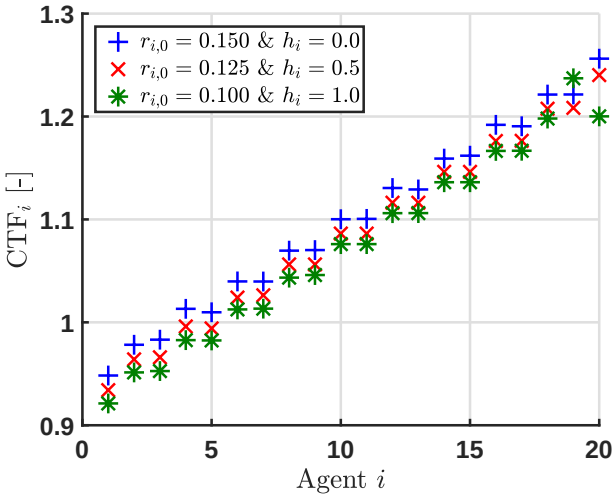

Figure 4.4: The CTF distributions for 20 with different spacing policy settings

Remark. *For $h_i = 1.0$ and $r_{i,0} = 0.1$, the CTF of agent 20 is lower than the CTF of agent 19. This indicates that agent 20 did merge in front of agent 19, while the trend is to merge behind agent 19. This deviation in merging order can as a side effect of the applied geometry and will be addressed in Section 4.7.*

To show that statement (ii) holds, animations and snapshots are made from the simulation with $h_i = 0$ and $h_i = 1$. For $h_i = 0$, the animation can be found at https://youtu.be/aPw9-NoApQE[3], with the corresponding snapshot in Figure 4.5a. The animation for $h_i = 1$ is at https://youtu.be/TwTAshc_TMo[4] with a snapshot from this animation in Figure 4.5b. The total length of the agents is significantly smaller if $h_i = 1$ than with $h_i = 0$. Furthermore, the working of social-ACC is clearly visible in Figure 4.5b. The agents before the road narrowing have a small comfort zone due to their low (queuing) velocity, whereas the downstream agents have a larger comfort zone than the agents in Figure 4.5a since their speed is above the desired speed due to the pushing effect of tailgaters.

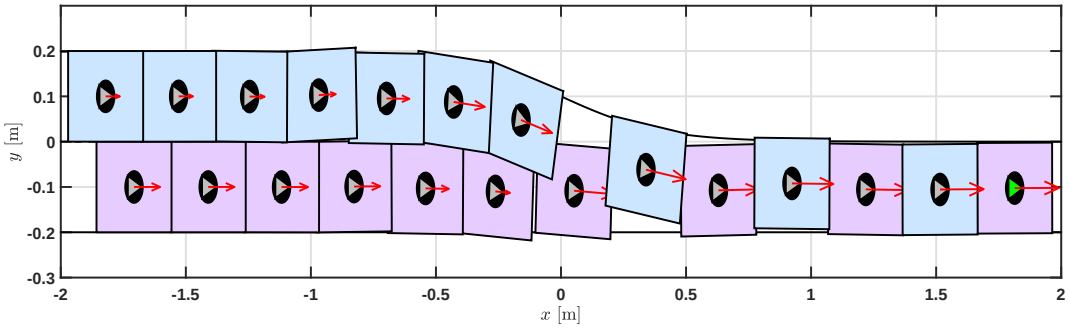

(a) Snapshot at $t = 129.1$ for $h_i = 0.0$ and $r_{i,0} = 0.15$

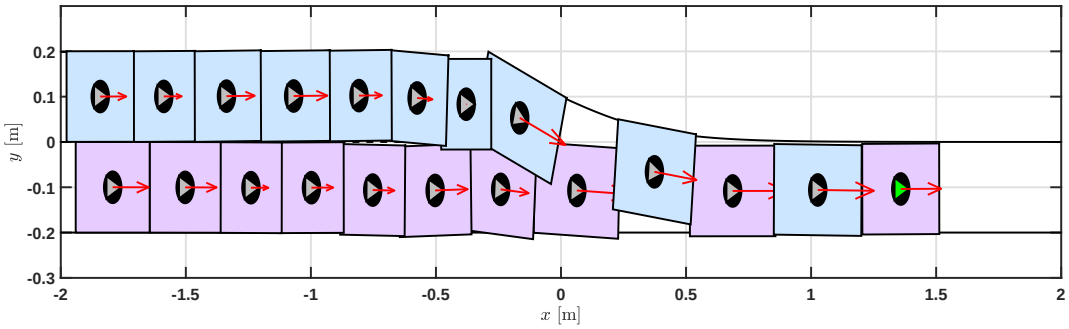

(b) Snapshot at $t = 119.3$ for $h_i = 1.0$ and $r_{i,0} = 0.10$

Figure 4.5: Snapshot from a simulation (a) without spacing policy and (b) with spacing policy. The velocity of each agent is indicated by the red vector.

4.4 Social-ACC versus 2D-ACC

The effect of social-ACC is investigated by comparing it with 2D-ACC. In 2D-ACC, an agent only reacts if another agent is in its comfort zone instead of the overlapping of two comfort zones. Furthermore the effect of tailgaters is neglected, while with social-ACC they are pushing each other through the road narrowing. The 2D-ACC strategy is elaborated in Section 3.3.

Comparing social-ACC with 2D-ACC, the following differences are observed:

i) social-ACC causes a major reduction of the CTF with respect to 2D-ACC;

ii) using larger headway times only causes a minor reduction with respect to the reduction caused by social-ACC;

[3] on the provided USB-stick listed as: `03_Lateral_geometry_without_spacing_policy.avi`.
[4] on the provided USB-stick listed as: `04_Lateral_geometry_with_spacing_policy.avi`.

iii) social-ACC increases the throughput (locally) at the road narrowing;

iv) using larger headway times increases the throughput before the road narrowing.

To substantiate these observations, the simulation results for 2D-ACC as well as social-ACC are shown. To distinguish the effect of 2D-ACC with the effect of the spacing policy, two different spacing policy settings from the previous section are used. Namely, $h_i = 1.0$ and $h_i = 0.5$ and their corresponding stand distances $r_{i,0} = 0.1$ and $r_{i,0} = 0.125$ respectively.

The average flow time and CTF of these simulations are shown in Table 4.8. There is a major difference between social-ACC and 2D-ACC, while there is only a minor difference visible between the used spacing policy settings. The average flow time and CTF of social-ACC are much lower than for 2D-ACC, indicating the advantage of social-ACC.

The CTF distribution, Figure 4.6, clearly shows that in 2D-ACC the agents are not pressurized by the upcoming agents since the CTF of the first agent is 1. The main difference between the CTF distributions is the average value, furthermore all distributions are very similar. Observation (i) and (ii) are substantiated since the average is mainly influenced by the choice of social-ACC, 2D-ACC or the headway time.

Table 4.8: The average flow time and CTF for 20 agents with social-ACC,2D-ACC and different headway times.

Setting:	h_i	0.5	1.0
	$r_{i,0}$	0.125	0.1
Average flow time	S-ACC	217.233	215.107
	2D-ACC	237.816	234.404
Average CTF	S-ACC	1.0862	1.0755
	2D-ACC	1.1891	1.1720

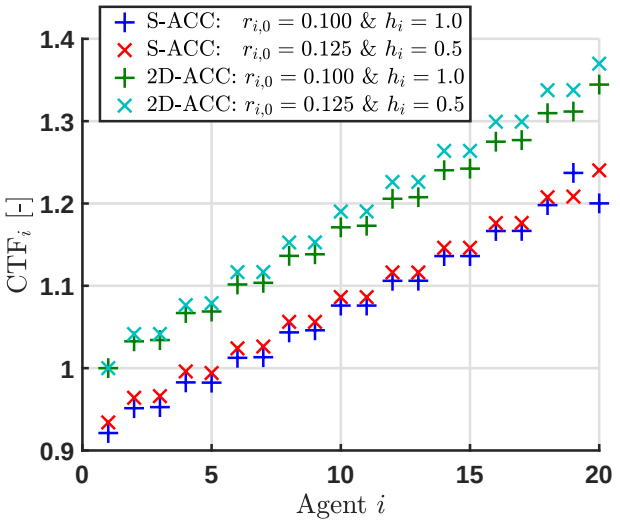

Figure 4.6: The CTF distributions for 20 agents equipped with social-ACC, 2D-ACC and different headway times.

Remark. *The effect of the headway time on social-ACC seems to be constant, while for 2D-ACC the CTF difference keeps increasing for agents further upstream. This effect is addressed in the next section.*

The throughput is shown in Figure 4.7. Before the road narrowing, the throughput is equal for all cases. Just before the road narrowing (at $x = -2$) where the throughput starts to reduce, a large difference is visible between the different headway times. Larger headway times result in a larger throughput since the agents need to slow down, consequently their comfort zone reduces. Since agents with a larger comfort zone can reduce their comfort zone further, a higher throughput is achieved, clarifying observation (iv).

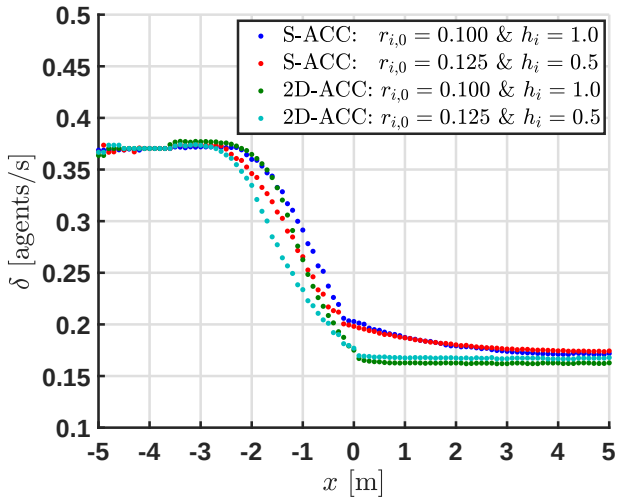

Figure 4.7: The throughput measured for a system of 20 agents equipped with social-ACC and 2D-ACC.

At the center of the road narrowing ($x = 0$), the main difference is caused by the interaction methods. With 2D-ACC the throughput is already at its final value, while with social-ACC the throughput reduces gradually to its new value. The gradual reduction of the throughput is the effect of social-ACC, agents are pushed through the road narrowing, causing them to minimize the inter-agent distance and drive above their desired speed, which clarifies observation (iii).

To give more insight in this effect, animations and snapshots are made from the simulation with $h_i = 1$. The animation of social-ACC can be found in the previous section (Figure 4.5b and at `https://youtu.be/TwTAshc_TMo`[4]). The animation of 2D-ACC is at `https://youtu.be/G6hgYCmu78Q`[5] with the corresponding snapshots in Figure 4.8.

Looking at the animations/snapshots it is clearly visible that agents with 2D-ACC are not pressurized since there are gaps between the comfort zones and the predecessor. This results in a lower throughput than with social-ACC, where the agents are forced to close the gaps due to the pushing. This clarifies the difference in throughput between 2D-ACC and social-ACC.

Furthermore, it can be seen that in both cases the agent are slowing down and their comfort zone decreases accordingly. Showing the cause of the increased throughput before the road narrowing for social-ACC as well as 2D-ACC.

However, to ratify the hypothesis from Chapter 3 "by taking the other agent's comfort zone into account, a more social behavior where agents make place for each other is induced, resulting in a better flow through the road narrowing", additional simulations are required. The observed difference in this section is mainly caused by the pushing effect of tailgaters. Therefore, the next chapter will focus on the effect of tailgaters and the main difference in working principle of 2D-ACC and social-ACC.

[4]on the provided USB-stick listed as: `04_Lateral_geometry_with_spacing_policy.avi`.
[5]on the provided USB-stick listed as: `05_2D-ACC_with_spacing_policy.avi`.

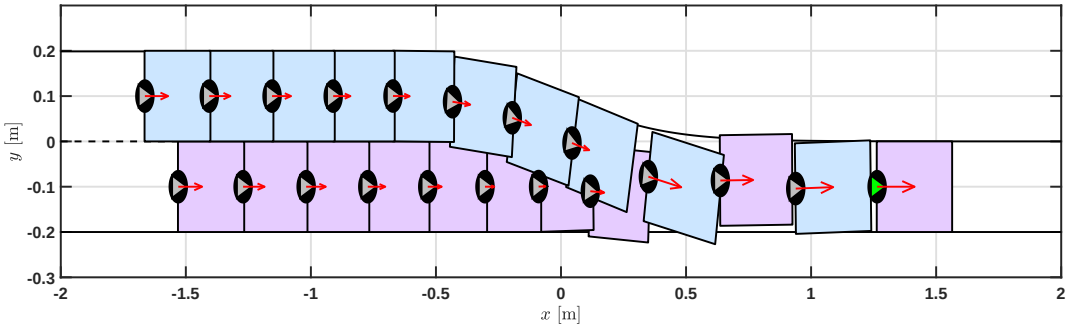

(a) $t_0 = 125.3$

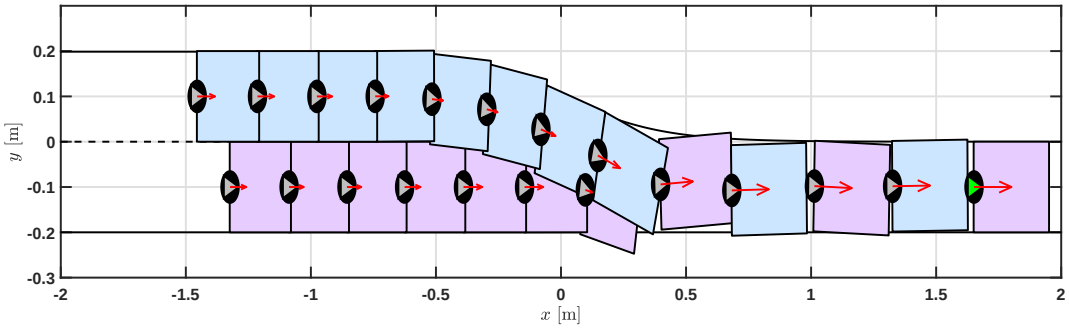

(b) $t_1 = 133.0$

Figure 4.8: Two snapshots from a simulation with 2D-ACC, $h_i = 1$ and $r_{i,0} = 0.1$. Note that the agents are now inside each others comfort zone, which is not the case with social-ACC. Furthermore, it can be seen that agents merge but after merging there is a gap between their comfort zones.

4.5 Reducing the pushing effect from tailgaters

The previous section essentially shows the advantage of social-ACC taking tailgaters into account, rather than the fundamental difference between social-ACC and 2D-ACC. Therefore, the focus of this section is on showing effect of reducing the pushing by tailgaters. The following observations are made by means of simulations:

i) reducing the pushing effect of tailgaters increases the average flow time significantly;

ii) without taking tailgaters into account, social-ACC has a fundamental advantage over 2D-ACC.

The effect of tailgaters is reduced by varying the back smoothing parameter $\xi_{b,i} \in [0, 1]$ and the length of the comfort zone at the back $\ell_{b,i}$. Recall that for $\xi_{b,i} = 0$ the back is completely smoothed and that $\xi_{b,i} = 1$ requires $\ell_{b,i} > r_i$ (see Section 3.2.1). The following social-ACC cases are compared to 2D-ACC: no reduction at all, thus $\xi_{b,i} = 1$ and $\ell_{b,i} = 2r_i$ which is identical to the interactions used in the previous section; completely smoothed by setting $\xi_{b,i} = 0$ and $\ell_{b,i} = r_i$; and a completely removed comfort zone at the back equal to 2D-ACC, $\xi_{b,i} = 0$ and $\ell_{b,i} = 0.01r_i$.

The effect of these cases on the average flow time and CTF is shown in Table 4.9. Reducing or removing the effect of tailgaters has almost the same effect as switching to the 2D-ACC strategy. However, the pushing effect of tailgaters is still visible since removing the complete comfort zone leads to a slightly lower flow time than with a reduced weighting.

Table 4.9: The average flow time and CTF of 20 agents with, without or a reduced pushing effect by tailgaters.

Setting:	$\xi_{b,i}$	1.0	0	0
	$\ell_{b,i}$	$2r_i$	r_i	$0.01r_i$
Average flow time	S-ACC	215.107	234.587	233.179
	2D-ACC	-	-	234.404
Average CTF	S-ACC	1.0755	1.1729	1.1659
	2D-ACC	-	-	1.1720

The CTF distributions are shown in Figure 4.9. Only a very subtle difference is visible between the removed and reduced effect, but there is a large difference with the case where the pushing effect of tailgaters is fully taken into account. This shows that observation (i) holds.

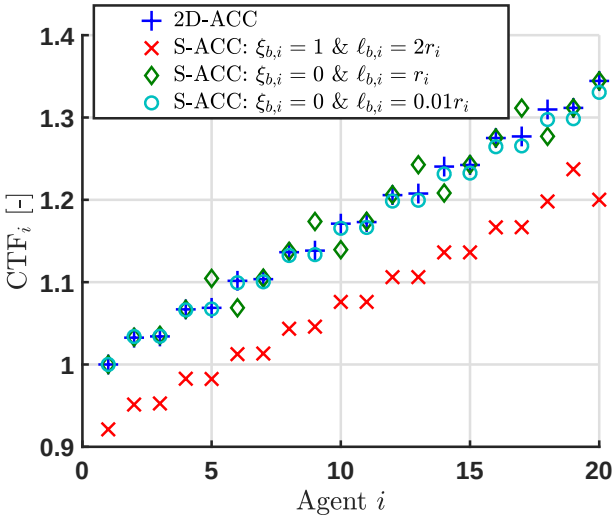

Figure 4.9: The CTF distributions for 20 agents with, without or a reduced pushing effect by tailgaters.

However, if the back of the comfort zone is smoothed ($\xi_{b,i} = 0$ & $\ell_{b,i} = r_i$) the agents do not merge alternately (other agents further upstream have a lower CTF indicating an overtake). This overtaking behavior is caused by excessive rotation of agents waiting at the road narrowing. This rotation creates enough space for other agents also to merge in front of the waiting agent. Therefore, the agents are merging groupwise instead of alternately. This behavior is shown in animation at `https://youtu.be/3ucD4Wu1YOg`[6] and in the snapshot in Figure 4.10. The rotating behavior is seen as a side effect of the changed geometry by reducing the back of the comfort zone. These effects are covered in Section 4.7.

Although, it is shown that observation (i) holds, observation (ii) cannot be confirmed with these simulations due to the small difference between the cases.

[6] on the provided USB-stick listed as: `06_Reduced_effect_from_tailgaters.avi`.

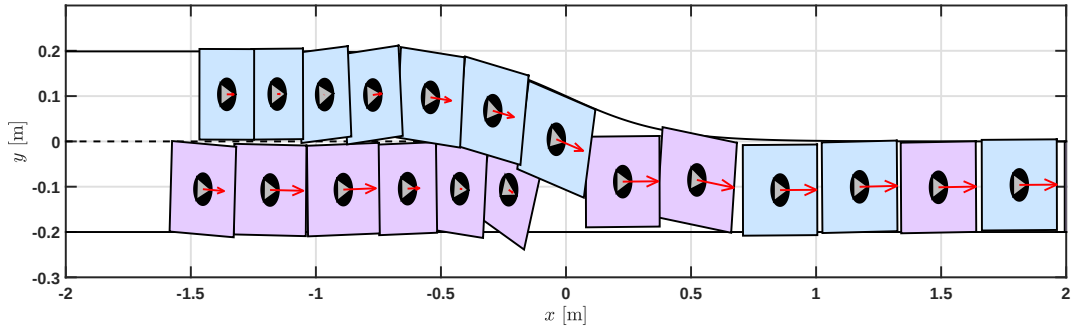

Figure 4.10: Snapshot from a simulation at $t = 142.9$ where the weighting of violation from behind is reduced, $\xi_{b,i} = 0$ & $\ell_{b,i} = r_i$. The agents do not close the gap between their comfort zones, since they do not experience an interaction force by tailgaters. Furthermore the agents do not merge alternately but groupwise due to excessive rotation.

The CTF distributions of simulations with 100-agents are shown in Figure 4.11. The displayed cases are social-ACC where the pushing effect by tailgaters is removed and 2D-ACC. For both cases the CTF settles to a constant value, thus the system eventually reaches a "steady-state". In this steady-state, the final CTF for agents with social-ACC is significantly lower than with 2D-ACC, indicating the advantage of social-ACC. Now, observation (ii) is also shown to be true.

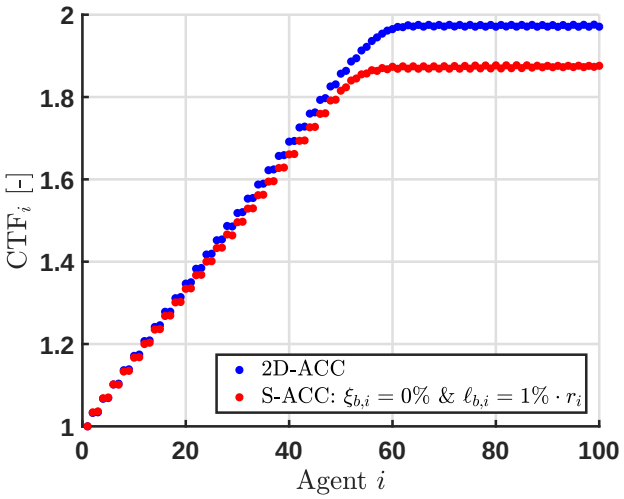

Figure 4.11: The CTF distribution for 100 agents equipped with 2D-ACC and social-ACC, neglecting the effect of tailgaters.

4.6 Speed saturation

In the previous sections it is shown that tailgaters force upstream agents to drive faster than the desired cruise speed. However, it may not be desirable that agents drive faster than their desired speed due to speed limitations. Therefore, the effect of a speed saturation is analyzed by means of simulations, resulting in the following observations:

i) the speed saturation limits the average flow time;

ii) social-ACC performs better with a speed saturation at the desired speed than 2D-ACC in general;

iii) a speed saturation will cause a (more) turbulent flow.

The agents increase their speed due to pushing upstream agents. Limiting the speed will cause a reduction of the flow time, which is shown in Table 4.10. The lower the speed limit, the larger the average flow time and CTF becomes.

Table 4.10: The average flow time and CTF of 20 agents with different speed limitations.

Setting:	$v_i^{\max}$	∞	$1.2 \cdot v_i^c$	$1.1 \cdot v_i^c$	v_i^c
Average flow time	S-ACC	215.107	218.395	222.242	229.888
	2D-ACC	234.404	-	-	-
Average CTF	S-ACC	1.0755	1.0920	1.1112	1.1494
	2D-ACC	1.1720	-	-	-

The CTF distributions are shown in Figure 4.12. Here it can be seen that the speed limit only shifts the average value of the CTF distribution and does not have any further effect. Furthermore, it is clear that social-ACC performs significantly better than 2D-ACC, even with a speed limit. This difference is caused by the pushing upstream agents, forcing other agents to minimize (and close) the gaps between comfort zones which arise during merging.

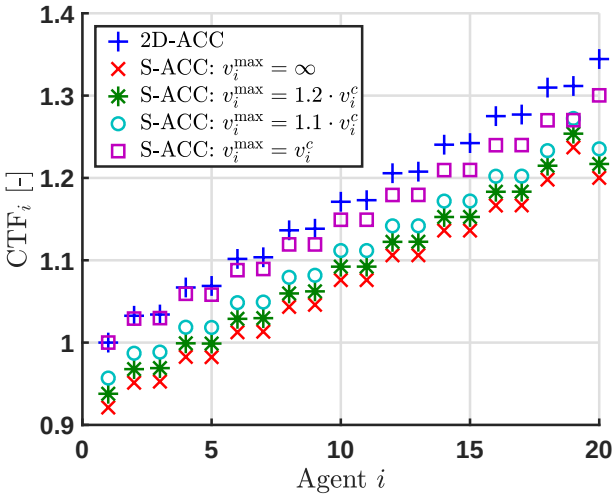

Figure 4.12: The CTF distributions for 20 agents with different speed limitations.

Since it is known (from the previous section) that the CTF for agents equipped with 2D-ACC will converge to a constant value, simulations with 100 agents are also performed for social-ACC. The average flow time and CTF obtained from these simulations are shown in Table 4.11 and the CTF distributions in Figure 4.13.

Table 4.11: The average flow time and CTF of 100 agents with different speed limitations.

Setting:	$v_i^{\max}$	∞	$1.2 \cdot v_i^c$	$1.1 \cdot v_i^c$	v_i^c
Average flow time	S-ACC	273.297	279.414	290.149	-
	2D-ACC	339.597	-	-	-
Average CTF	S-ACC	1.3665	1.3971	1.4507	-
	2D-ACC	1.6980	-	-	-

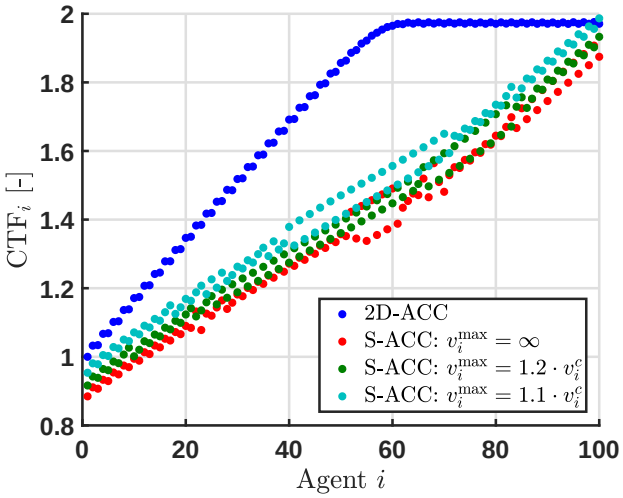

Figure 4.13: The CTF measured for agent 100 with different speed limitations.

In Figure 4.13 it can be seen that for 100 agents the CTF does not converge to a constant value. Instead of converging, the CTF distributions shows some outliers, indicating that multiple agents have made an overtake.

The overtaking is caused by the increasing pressure of the upstream agents pushing the predecessors. This is shown in the animation at `https://youtu.be/QxOLvxCf0ZU`[7] and the corresponding snapshot in Figure 4.14. This animation/snapshot shows that the pressure created by the pushing upstream and blocking downstream agents causes agents to shift in their lane and rotate excessively. Hence, a "turbulent" flow emerges.

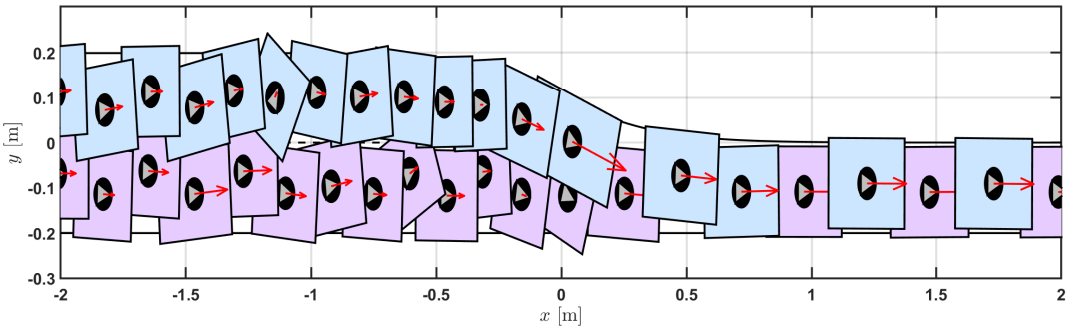

Figure 4.14: Snapshot at $t = 271.0$ from a simulation with 100 agents and no speed saturation. A turbulent flow emerges due to the pushing agents upstream and blocking agents downstream.

[7] on the provided USB-stick listed as:
`07_100_agents_with_lateral_geometry_and_no_speed_saturation.avi`.

The flow becomes more turbulent if the speed limit is lowered. To show this, the mean of $||\sigma_i||_{\mathcal{L}_2}$ and mean$||\omega_i||_{\mathcal{L}_2}$ is used. The $\mathcal{L}_2$-norm is defined by taking the integral from $t = 0$ to $t = \infty$, which is possible since all signals (eventually) converge towards zero and the simulation is terminated if all signals are close to zero. Hence, taking the integral over the obtained simulation span equals the integral to $t = \infty$.

Steering results in orientations changes, which create a "turbulent" flow, while a "laminar" flow is desired for the sake of comfort. By taking the average steering energy $||\omega_i||_{\mathcal{L}_2}$ over all agents, it is determined how turbulent the flow of agents is. The same holds for $||\sigma_i||_{\mathcal{L}_2}$, which indicates the experienced stress energy of an agent. The stress indicates the chance that an agents suddenly experiences a large force and "shoots" away from the current structure. Since this is undesired behavior, the amount of stress energy should be low.

From Table 4.12 it can be concluded that the saturation increases the turbulent flow slightly since both measurement increase slightly. The turbulent flow is mainly caused by the larger number of agents present in the system, since for a system of 20 agents without saturation mean$||\sigma_i||_{\mathcal{L}_2} = 40.12$ and mean$||\omega_i||_{\mathcal{L}_2} = 7.809$.

Table 4.12: The average stress for 100 agents with different speed limitations.

Setting:	$v_i^{\max}$	∞	$1.2 \cdot v_i^c$	$1.1 \cdot v_i^c$	v_i^c
mean $||\omega_i(t)||_{\mathcal{L}_2}$	S-ACC	12.134	12.358	12.697	-
	2D-ACC	2.041	-	-	-
mean $||\sigma_i(t)||_{\mathcal{L}_2}$	S-ACC	178.031	183.093	198.531	-
	2D-ACC	13.591	-	-	-

4.7 Additional comfort zone geometry

In the previous sections it is shown that changing some parameters or increasing the number of agents can cause some side effects. Examples for these side effects are excessive rotation or (extremely) larger interaction forces. These effects are mainly caused by the application of geometry to the circular comfort zone, where $\xi_{w,i}$ and $\xi_{b,i}$ have the largest influence. This section will illustrate the following observations regarding the the different parameters and geometry:

i) increasing the lateral smoothing decreases the CTF and chance on a turbulent flow;

ii) the effect of additional geometry heavily dependent on the lateral stiffness.

iii) reducing the effect of tailgaters lowers the stress and rotation energy, thus less chance on a turbulent flow, but increases the flow time;

The four types of geometry which will be discussed are covered in Section 3.2. There will be referred to these comfort zone geometries as shown in Table 4.13.

Table 4.13: Geometry naming and reference to their visualization.

Name	**Visualization**
No geometry	Figure 3.8
Point front	Figure 3.9a
Point back	Figure 3.9b
Two points	Figure 3.9c

4.7.1 Lateral comfort zone stiffness

First, the effect of the lateral comfort zone stiffness is investigated for the different geometries. The lateral comfort zone stiffness is mainly determined by the smoothing function Ψ. Changing the parameter $\xi_{w,i} \in [0, 1)$ determines the amount of lateral smoothing.

In general, the more the comfort zone is smoothed, the lower the CTF becomes (shown in Figure 4.15). Since the interaction from the sides is limited, the agents experience lower force perpendicular to their orientation, resulting in less rotation. This effect is clearly visible in Figure 4.15. The agents experience less stress overall, due to the smoothing, see Figure 4.16b. However, certain combinations of geometry and smoothing can result in a turbulent flow.

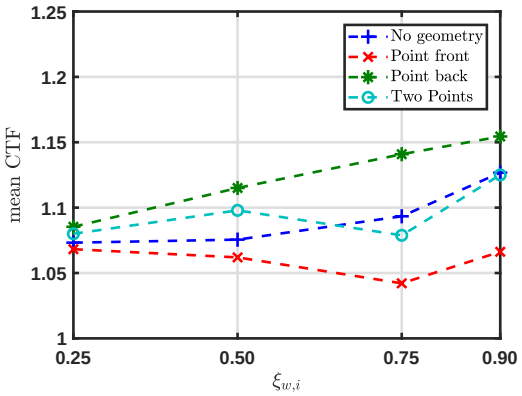

Figure 4.15: The mean CTF for 20 agents with different lateral smoothing and comfort zone geometries.

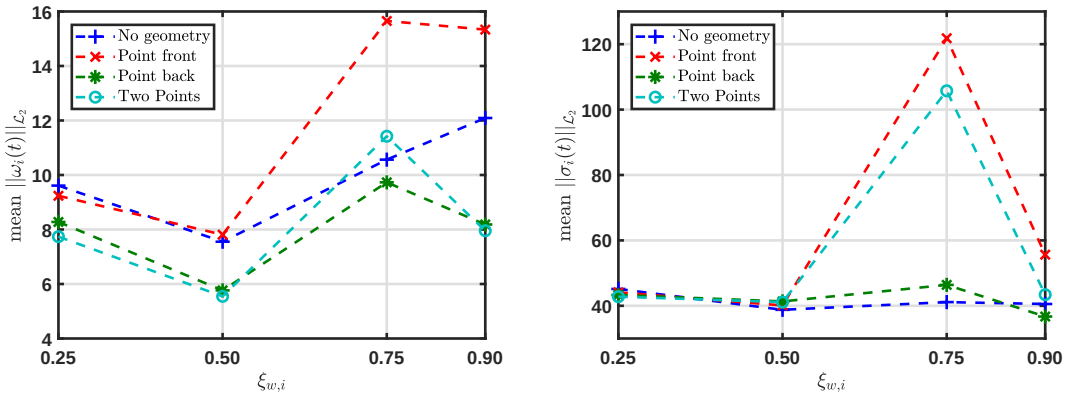

(a) Rotation

(b) Stress

Figure 4.16: The mean (a) rotation and (b) stress for 20 agents with different lateral smoothing and comfort zone geometries.

At first sight, there is no direct link between the used geometry, lateral stiffness and the emergence of a turbulent flow. However, the excessive rotation for a geometry can be clarified. The excessive rotation is mainly caused by comfort zone violation diagonally behind the agent. This violation will cause the agent to rotate away from the point of violation, creating an undesired movement towards the boundary which has to be corrected. If the geometry has a small or smooth comfort zone at the back (e.g. point), while having an equally or larger comfort zone at the front, the rotation is limited since the generated interaction forces cancels the rotation. However, if the agent's comfort

zone is larger or stiffer at the back than at the front, more rotation is created since the forces do not cancel each other. The boundary delivers a lower force than the violating agent, causing the agent to rotate towards the boundary. This increases the interaction force, causing even more rotation until the boundary delivers a sufficiently large force to cancel it.

This effect is shown in the animation and snapshot of the simulation resulting in the most turbulent flow (geometry: point front; $\xi_{w,i} = 0.75$). The animation is at https://youtu.be/Pv2rqdKDP2U[8] and the corresponding snapshot in Figure 4.17. Only a bit of violation of the comfort zone at the back causes the agents to rotate towards the boundary, resulting in large interaction forces.

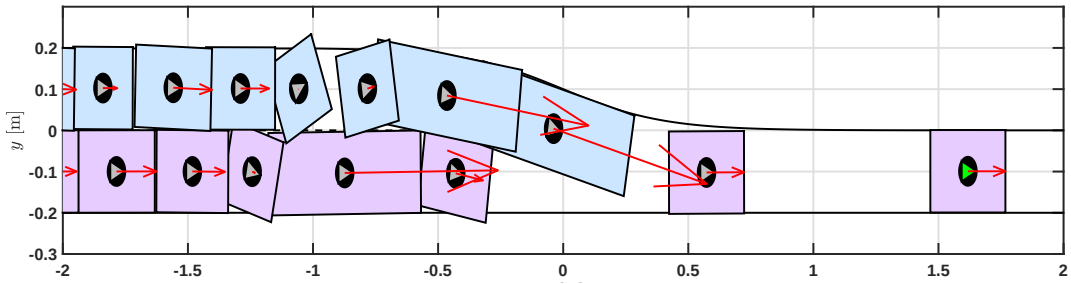

Figure 4.17: Snapshot at $t = 101.5$ from the simulation where the geometric comfort has a point at the front and $\xi_{w,i} = 0.75$. It can be seen that the agents are rotating too much and the velocity difference between agents is large.

4.7.2 Reducing the effect of tailgaters

The second parameter which will be studied for the different geometries, is the back smoothing factor $\xi_{b,i} \in [0, 1]$. The effect of the back smoothing factor $\xi_{b,i}$ is partially discussed in Section 4.5. This section continues on this by extending it to different geometries and a larger set of values for $\xi_{b,i}$.

Smoothing the indicator function at the back results in increasing CTF and reduces the stress and rotation (shown in Figures 4.18 and 4.19) The rotation reduction is geometry independent due to the previously explained effect. In these figures the trade off between performance and comfort is also clearly visible.

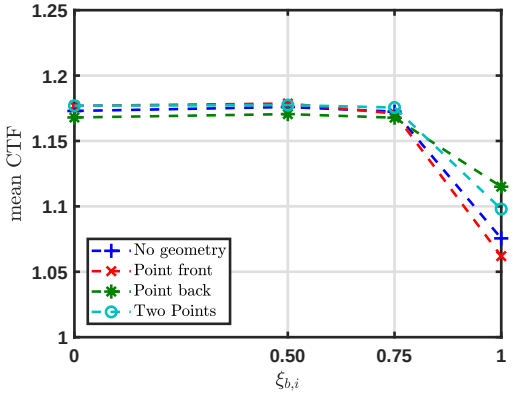

Figure 4.18: The mean CTF for 20 agents with different comfort zone geometries and back smoothing factors.

[8] on the provided USB-stick listed as: `08_Point_at_front_geometry.avi`.

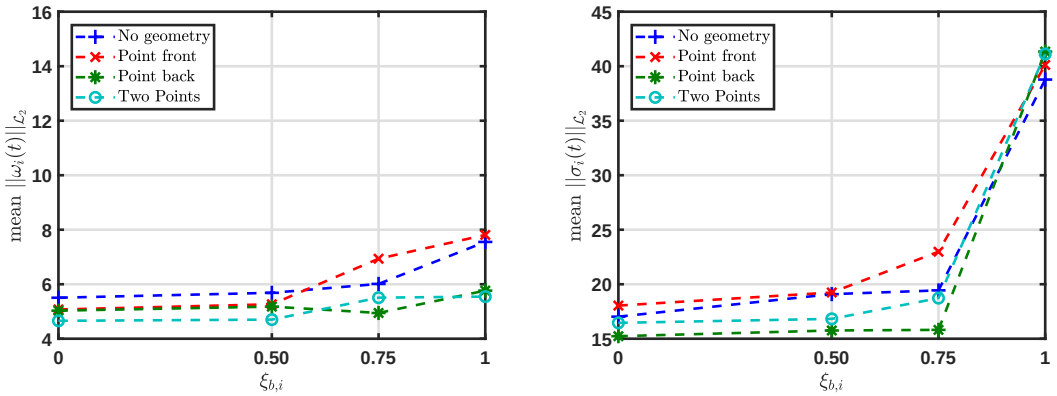

(a) Rotation (b) Stress

Figure 4.19: The mean (a) rotation and (b) stress for 20 agents with different comfort zone geometries and back smoothing factors.

4.8 Summary of simulation results

If the agent's constraints are not considered in an appropriate way, it can have a tremendous effect. It is shown that a non appropriate linking between the social force model and the agent kinematics can result in unstable behavior. Emphasizing the importance of taking constraints into account.

The further focus of this chapter was on characterizing the effect of the interaction design on the performance (flow time and throughput) and collective behavior (fluent merging / laminar flow). In general, social-ACC with its current interaction rules increases the performance, but also increases the rotation of agents eventually resulting in a turbulent flow. This turbulent flow is mainly caused by violation of the comfort zone diagonally behind the agent causing the agent to rotate away and thereby increasing the violation.

An overview of social-ACC, 2D-ACC and the different implemented features with their corresponding effect on the performance and collective behavior is given in Table 4.14. The excessive rotation is mainly caused by the addition of geometry to the interaction rules.

Table 4.14: An overview of the different methods and implemented features and their corresponding effect on the performance (flow time and throughput) emergence of a turbulent flow (rotation). A major positive effect is indicated by $++$, a minor positive effect by $+$, a neutral effect by $+/-$ effect, a major and a minor negative effect with $--$ and $-$ respectively.

	Performance	**Rotation**
2D-ACC	$+/-$	$+/-$
S-ACC	$++$	$--$
Geometry	$--$	$--$
Comfort zone overlap	$++$	$+-$
Larger headway times	$+$	$-$
Effect of tailgaters	$++$	$--$
Speed limitations	$-$	$-$

Chapter 5

Alternative interaction design

In the previous chapters a circular comfort zone was considered first, resulting in an average CTF close to 1. To maintain the same measure of violation but also taking care of the road geometry, the smoothing function was added. This resulted directly in a larger average CTF and more rotation, resulting in the possibility for a turbulent flow to emerge. The turbulent flow can emerge due to a rapidly increasing interaction force if the side of the comfort zone is violated, despite the applied smoothing.

Another cause of the turbulent flow is the pressure of a large number of agents. Due to the circular comfort zones agents will push each other such that they shift in their lane, which will cause violation at the side of the comfort zone, again resulting in a turbulent flow. Therefore it may be beneficial not to use the circular comfort zones to determine the violation but another geometry.

Consider that each agent $i \in \mathcal{V}$ has a rectangular comfort zone with width $\omega_{c,i}$. The length of the comfort zone, measured from the agent to the front is $\ell_{f,i}$, while the length to the back of the comfort zone is $\ell_{b,i}$, creating a total length of $\ell_i := \ell_{b,i} + \ell_{f,i}$. This rectangular comfort zone is visualized in Figure 5.1. The spacing policy can also be added by $\ell_{f,i} = \ell_{f_0,i} + h_i||\mathbf{v}_i||$, which is applied to the back.

Due to the square comfort zone, it is not possible to take the same measure of violation as with circular comfort zones (3.2) since the new comfort zone is not axisymmetric. Hence, a different geometry requires a different measure of violation. This chapter will discuss two different measures of violation for rectangular comfort zones.

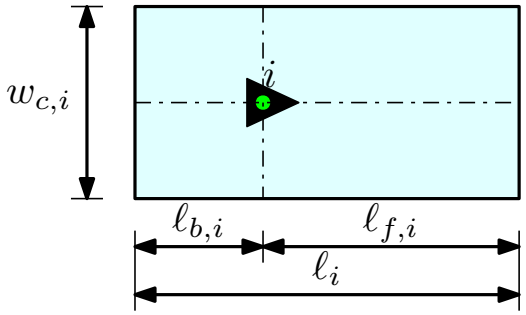

Figure 5.1: The rectangular comfort zone with the corresponding dimensions.

5.1 The distance to the other agent's comfort zone

Using circular comfort zones, the inter-agent violation is measured by taking the overlap of the two comfort zones. This measure indicates how far the comfort zone of agent j is inside the comfort zone of agent i and vice versa. To apply a similar measure for

rectangular comfort zones, the measure is split up in a longitudinal and lateral measure of violation.

A vector from agent i to the closest point of the comfort zone of agent j is denoted as $\tilde{\mathbf{d}}_{ij} = \begin{pmatrix} \tilde{d}_{ij,x} & \tilde{d}_{ij,y} \end{pmatrix} \mathbf{e}^i$, which is expressed in the local agent frame. The violation in the longitudinal direction is then

$$g_{ij,x} := \begin{cases} \frac{\ell_{b,i} + \tilde{d}_{ij,x}}{\ell_b} & \text{if } \tilde{d}_{ij,x} < 0 \\ \frac{\ell_{f,i} - \tilde{d}_{ij,x}}{\ell_f} & \text{if } \tilde{d}_{ij,x} \geq 0 \end{cases}$$

and in the lateral direction

$$g_{ij,y} := \begin{cases} \frac{\frac{1}{2} w_{c,i} + \tilde{d}_{ij,y}}{\frac{1}{2} w_{c,i}} & \text{if } \tilde{d}_{ij,y} < 0 \\ \frac{\frac{1}{2} w_{c,i} - \tilde{d}_{ij,y}}{\frac{1}{2} w_{c,i}} & \text{if } \tilde{d}_{ij,y} \geq 0 \end{cases}.$$

Those two measures of violation should be reduced to one measure since the social force framework requires a scalar indicating the violation. Creating a scalar measure of violation from the two earlier derived measures, can be achieved in many ways. A possibility is to apply a weighting to the longitudinal and later violation, $k_{x,i}$ and $k_{y,i}$ respectively, and sum both measures

$$g_{ij} := \frac{\ell_{f,i}}{k_{x,i} + k_{y,i}} \cdot \begin{pmatrix} k_{x,i} & k_{y,i} \end{pmatrix} \begin{pmatrix} g_{ij,x} \\ g_{ij,y} \end{pmatrix},$$

while another possibility is to take the product

$$g_{ij} := \ell_{f,i} \cdot g_{ij,x} \cdot g_{ij,y}. \tag{5.1}$$

The product measure requires an additional multiplication of the comfort zone length, to create a similar weighting as in (3.2). The original and new weighting methods are visualized in Figure 5.2.

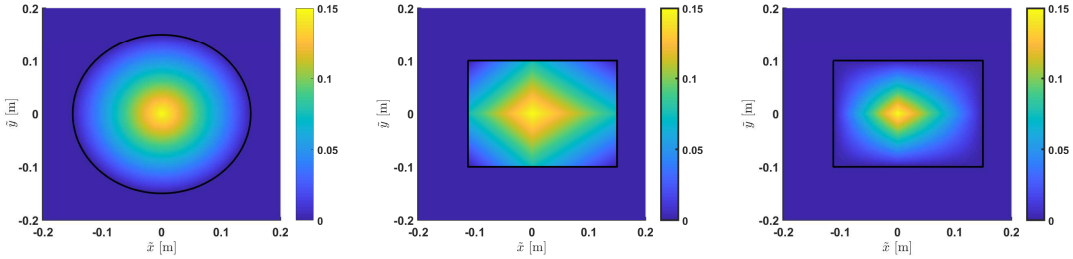

(a) (b) (c)

Figure 5.2: Different violation functions (a) the original violation for circular comfort zones, (b) the geometric violation with summation weighting and (c) the geometric violation with product weighting.

For the completeness of this interaction design, the interaction function needs to be defined. The interaction function is defined as the indicator function

$$\Upsilon_{ij} := I_{ij}.$$

The indicator is 1 if the closest point of agent j's comfort zone to agent i is inside the comfort zone of agent i. The closest point of agent j's comfort zone to agent i is the

point M_{ij}. Thus, it can be derived that

$$I_{ij} := \begin{cases} 1 & \text{if } (0 \leq \mathbf{C}_{1,i}\mathbf{M}_{ij} \cdot \mathbf{C}_{1,i}\mathbf{C}_{2,i} \leq \mathbf{C}_{1,i}\mathbf{C}_{2,i} \cdot \mathbf{C}_{1,i}\mathbf{C}_{2,i}) \wedge \dots \\ & \quad (0 \leq \mathbf{C}_{1,i}\mathbf{M}_{ij} \cdot \mathbf{C}_{1,i}\mathbf{C}_{4,i} \leq \mathbf{C}_{1,i}\mathbf{C}_{4,i} \cdot \mathbf{C}_{1,i}\mathbf{C}_{4,i}) \\ 0 & \text{otherwise} \end{cases}$$

with corner points $\mathbf{C}_{1-4,i}$. The term $\mathbf{C}_{1,i}\mathbf{M}_{ij}$ denotes the vector pointing from $\mathbf{C}_{1,i}$ to $\mathbf{M}_{1,i}$. The corner points are defined as shown in Figure 5.3.

The environmental interactions are similar to the inter-agent interactions, but agent j is replaced by obstacle W and the closest point of the other agent's comfort zone is replaced by the most effective point of violation $\hat{\mathbf{x}}$

$$\hat{\mathbf{x}} := \arg \max_{\mathbf{x} \in \mathcal{W}_W} \left(\Upsilon_{iW}(\mathbf{p}_i, \mathbf{v}_i, \mathbf{x}) g_{iW}(\mathbf{p}_i, \mathbf{v}_i, \mathbf{x}) \right).$$

Independent from the weighting method, this unstable behavior is observed. This indicates that the defined measure of violation is not appropriate. Therefore, the measure of violation is visualized in Figure 5.3.

Here it can be seen that agent j only experiences a bit violation while agent i experiences a lot of violation. Hence, agent i will experience a relatively large force while agent j will experience a smaller force. This is in contrast with intuition, where agent j should experience the largest force and decelerate while agent i should only accelerate a bit. The measure of violation is thus inappropriate, and a different measure is required.

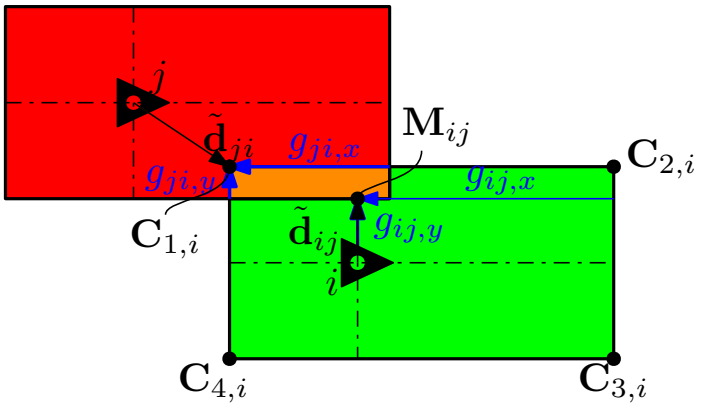

Figure 5.3: The closest point of the agent to the other agent's comfort zone is denoted as $\mathbf{M}_{ij}$ pointed at by black vector $\tilde{\mathbf{d}}_{ij}$, while the weighting based on this point is visualized by the blue vectors $g_{ij,x}$ and $g_{ij,y}$.

5.2 The comfort zone intersection area

Another method to determine the inter-agent violation is by using the overlapping comfort zone area as interaction and violation function. Assume that the location, geometry and orientation of the comfort zone of agent i is described by the set $\mathfrak{C}_i$. There is interaction between the two agents if the comfort zone of agent i and j overlap. Therefore, the interaction function is defined by the indicator function

$$\Upsilon_{ij} := I_{ij}, \tag{5.2}$$

and the indicator function is 1 if the intersection set of the two comfort zones is not empty

$$I_{ij} := \begin{cases} 0 & \text{if } \mathfrak{C}_i \cap \mathfrak{C}_j = \emptyset \\ 1 & \text{otherwise} \end{cases}. \tag{5.3}$$

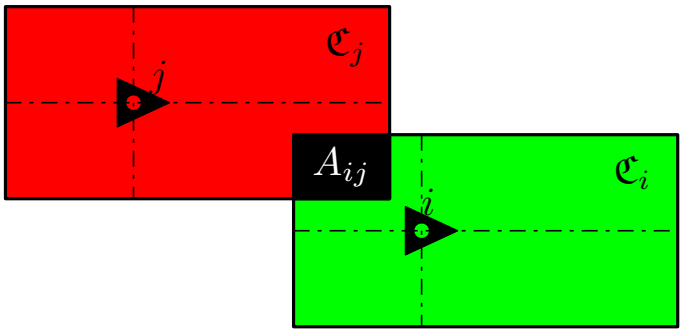

Figure 5.4: Visualization of the comfort zone intersection area.

The violation is set equal to the overlapping area

$$g_{ij} := A_{ij} = A_{ji},$$

which is visualized in Figure 5.4.

The environmental interactions are equal to the interactions defined in social-ACC (see Section 3.2.2), with comfort zone lengths $\ell_{f,i} = \ell_{b,i} = r_i = r_{i,0} + h_i||v_i||$. All further settings are equal to the earlier used settings in Table 4.3.

Multiple simulations are performed with an increasing number of agents $n \in \{2, 4, 8, 20\}$. The simulations with this method are rather successful, since the agent's are merging faster and more fluently than with the earlier defined interactions.

The faster merging is clearly visible when looking to the average flow time and CTF of a simulation with 20 agents in Table 5.1. The average CTF value is much closer to 1 than the average CTF of agents where geometry is added to the circular comfort zones. The CTF distribution is shown in Figure 5.5, which is very similar to the CTF distribution of the circular comfort zone without geometry.

Table 5.1: The average flow time and CTF for 20 agents with the area violation measure.

Setting	**Area weighting**
Average flow time	206.464
Average CTF	1.03232

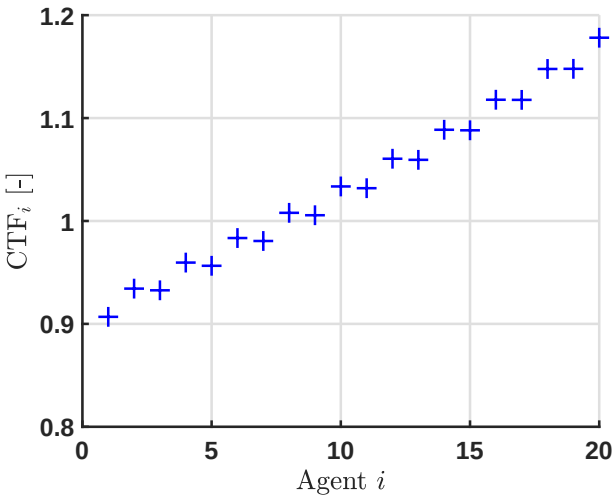

Figure 5.5: The CTF distribution for 20 agents with the area violation measure.

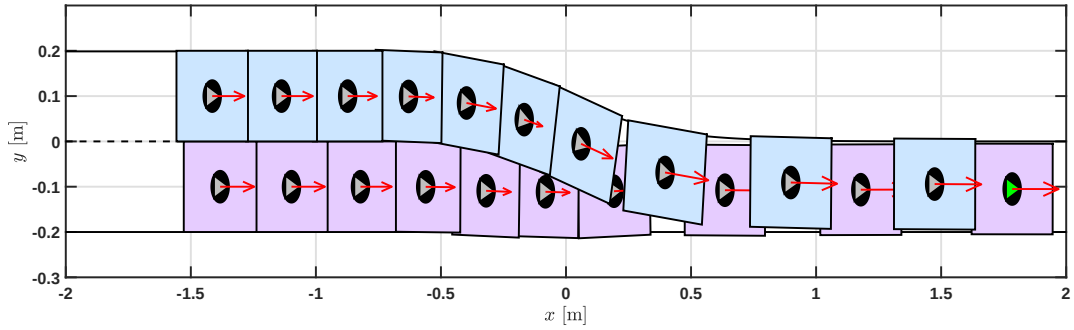

Figure 5.6: Snapshot at $t = 126.9$ from the simulation with the area violation measure. The agents merge fluently but have more comfort zone overlap than with other methods.

In the animation and snapshot of this simulation it is also clearly visible that the agents merge very fluently. The animation of this simulation can be found at `https://youtu.be/yMkVUpVQX2I`[1] and the corresponding snapshot in Figure 5.5.

Although, the agents merge very fluently, the comfort zones overlap more than with the other methods. This indicates that it less stiff than the earlier used methods. Since it is known from the previous chapter that increasing stiffness can cause more rotation, an additional gain parameter for the area weighting should be introduced and analyzed.

Although the simulation results look promising, this method also has a disadvantage. With the area method multiple scenarios can result in the same weighting while a different weighting is desired. E.g. it could be desired to take comfort zone violation from behind less into account than violation at the front or at the side of the agent. With the area method these different scenarios can have the same intersection area, resulting in a similar weighting while a different weighting is desired (see Figure 5.7). Hence, the policy lacks tunability to let the violation dependent on the location of violation.

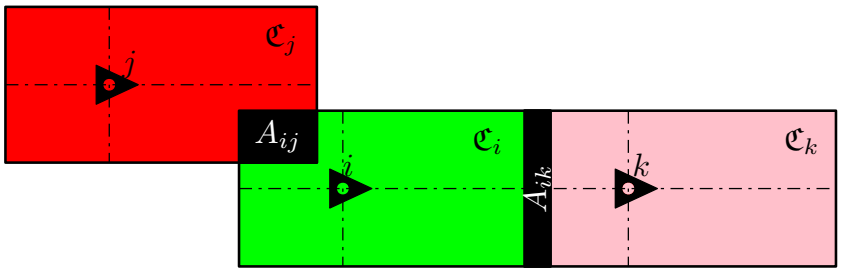

Figure 5.7: Two violation scenarios with the same weighting.

Another disadvantage could be the symmetry within the experienced inter-agent interaction forces. Since the intersection area is the same for both agents $A_{ij} = A_{ji}$, thus both agents experience the same violation. Therefore, both agents also experience the same force but in the opposite direction. This could result in a scenario where the agent are locked since all force are similar. Hence, an appropriate measure of violation still needs to be found.

[1] on the provided USB-stick listed as: `09_Area_violation.avi`.

Chapter 6

Conclusions and recommendations

The goal of the thesis is to create a control strategy for autonomous (highway) driving based on interaction rules, where the desired (collective) behavior emerges from the (local) interaction rules. Here, highway driving includes lane keeping; driving at a desired speed or (safe) distance to its predecessor; and merging. The road narrowing scenario is selected as a test case to measure the performance of the new strategy.

This chapters summarizes the conclusions of this thesis and provides recommendations for future research.

6.1 Conclusions

To study the effect of the interaction rules on the (collective) behavior it is important to take the agents' dynamics into account. Linking the already existing social force model to the unicycle kinematics by rewriting the nonholonomic constraint can result in unstable behavior. The forward velocity is directly set to the desired velocity magnitude without taking the orientation into account. Therefore, it is possible that the agent drives in the wrong direction, increasing the desired control action, resulting in unstable behavior. An appropriate linking between the social force model and the agent kinematics is made by taking the projection of the desired acceleration on the agent's orientation and translating it to the desired inputs, resulting in stable behavior. This shows the importance of taking the agents' dynamics into account, in particular their constraints.

The interaction rules of the social force model distinguish themselves from other models by taking the other agents' comfort zone into account. If two comfort zones overlap, both agents experience an interaction force. Doing so, anticipation is implicitly added to the model, resulting in collaboration between agents without requiring communication. An agent whose comfort zone is violated at the back will have the tendency to drive faster while the succeeding agents will slow down. In the road narrowing scenario this results in agents pushing each other through the road narrowing. The effect is measured by the flow time of each agent and the throughput. Due to the pushing effect, the average flow time of the agents is close to the nominal flow time. The first agents their flow time is lower than the nominal flow time since these agents are subject to the pushing, therefore driving faster than their desired speed. The first agents slow down the succeeding agents, consequently these agents have a higher flow time than the nominal flow time. However, the average flow time is close to the nominal flow time since all agents undertake an action: increasing or decreasing their speed. Hence, the agents share discomfort and collaborate to achieve a better flow through the road narrowing. Therefore, this method is called social-ACC.

However, for highway driving, the road geometry should be taken into account. By employing a 2D-bump function to filter the inter-action forces, geometry is added to the initial circular comfort zones. This addition of geometry resulted in a major performance reduction, while causing a turbulent flow through the road narrowing. Although, the bump functions smooths the interaction forces, the force created by violation diagonally behind the agent causes the agent to rotate. This rotation increases the violation until the boundary delivers a sufficiently large force to cancel the rotation. Resulting in a turbulent flow, which is the main problem of the current implementation of social-ACC.

However, a minor performance improvement can be made by implementing the constant time spacing policy such that agents only use the required amount of road. The spacing policy makes the size of the agents' comfort zone speed depending, such that the radius scales linear with the speed. A headway time results in slight reduction of the average flow time.

To compare the performance of social-ACC, ACC has been implemented in the social force model, which is called 2D-ACC. With this 2D-ACC, an agent experiences an interaction force if another agent is inside the comfort zone instead of the comfort zone overlap used in social-ACC. Comparing social-ACC and 2D-ACC, social-ACC has a significantly lower average flow time. The comfort zone overlap used in social-ACC causes agents to interact earlier, creating a kind of anticipation. With 2D-ACC the agent only reacts if the other agent is already inside its comfort zone, resulting in a more "egoistic" driving behavior. An agent cuts-off other traffic and force itself to merge between other agents, resulting in larger control actions for the succeeding agent. While testing different settings (e.g. headway time and reducing the effect of tailgaters), social-ACC always performed better than 2D-ACC. Hence, the social force model increases the performance, without the requirement of communication and/or a supervisory controller. However, social-ACC also created a more turbulent flow and sometimes a less fluent merging behavior due to the implementation of geometry.

One of the advantages of circular comfort zones is the isotropic measure of violation. As soon as geometry is introduced, it is hard to find an appropriate measure of violation. The measure of violation should be a scalar based on both agents' comfort zone since this is the working principle of the social force model. In addition, the appropriate agent should experience the largest force (i.e. violation), since it is more likely that the agent at the front or on the not removed lane undertakes equal or less action than a merging or succeeding agent. Consequently, not doing so, results in a more turbulent flow. An example of measuring the violation is by determining the area of the overlap, however this could result in different scenarios where the overlap is equal, but the desired interaction force should not.

Although the appropriate interactions are not found for geometric geometric comfort zones, the social force model (or social-ACC) has shown its potential for autonomous driving based on local interaction rules. With the social force model, it is possible to let agents drive in the desired direction; avoid collisions; merge; and locally improve the throughput. This is all achieved without the use of communication or supervisor.

Despite the fact these interaction rules may not be suitable for highway driving due to the emergence of a turbulent flow, it can be used in wide ranges of applications where there is more space available. If the agents have more room to deviate from their desired path, the interaction force are quickly reduced resulting in a more laminar flow of agents. Due to the use of simple local interaction rules, the agents can solve a wide variety of scenario's, without the requirement of prior knowledge, supervisory controller or communication. Hence, this solution can be used in a wide range of application such as autonomous transportation tasks in warehouses, harbors, factories etc..

6.2 Recommendations

The main problem with the current social-ACC is the emergence of a turbulent flow due to the inclusion of geometric constraints. The turbulent flow is caused by the excessive rotation, originating from violation of the comfort zone diagonally behind the agent. Resulting in rotation, increasing the interaction force and rotation. To tackle this problem, it may be beneficial to add an additional comfort zone to determine the agent movement. The largest comfort zone should be used to change the agent speed, while a smaller comfort zone is used to create rotation for collision avoidance. Doing so will result in the agent first trying to create a gap for the merging agent. If the other agents come to close, the additional comfort zone will cause the agent to change its orientation and avoid a collision.

Furthermore, a new measure of violation should be created which can deal better with the geometry. The area of the overlapping comfort zones, obtained by integrating over the intersection domain

$$\iint_{\mathfrak{C}_i \cap \mathfrak{C}_j} 1 \, dA,$$

has shown to be a useful measure since the effect is similar to circular comfort zones. Here $\mathfrak{C}_i$ and $\mathfrak{C}_j$ describes the geometry and location of agents i and j's comfort zone respectively. However, this method lacks weighting of the violation location (e.g. for equal areas, violation at the back should have a lower impact than violation at the front). Therefore, a location depending weighting should be added to the area integral

$$\iint_{\mathfrak{C}_i \cap \mathfrak{C}_j} \rho(\tilde{x}_i, \tilde{y}_i) \, dA.$$

Here $\tilde{x}_i e_1^i + \tilde{y}_i e_2^i = \begin{pmatrix} \tilde{x}_i & \tilde{y}_i \end{pmatrix} \mathbf{e}^i$, which are the agent's local (x, y)-coordinates. E.g. the weighting is split into a lateral and longitudinal term $\rho(\tilde{x}_i, \tilde{y}_i) = \rho_x(\tilde{x}_i)\rho_y(\tilde{y}_i)$. Consider the longitudinal density function

$$\rho_x(\tilde{x}_i) := \begin{cases} \delta_f \left(-\frac{\tilde{x}_i}{\ell_f} + 1 \right) & \text{if } 0 \leq \tilde{x}_i \leq \ell_f \\ \delta_b \left(\frac{\tilde{x}_i}{\ell_b} + 1 \right) & \text{if } -\ell_b \leq \tilde{x}_1 < 0 \\ 0 & \text{otherwise} \end{cases}.$$

Where the agent is centered at $\begin{pmatrix} \tilde{x}_i & \tilde{y}_i \end{pmatrix} = \begin{pmatrix} 0 & 0 \end{pmatrix}$ and ℓ_f, ℓ_b are the comfort zone lengths at the front and back respectively. Furthermore, the parameters δ_f, δ_b determine the weighting at the front and back respectively. Setting $\delta_f > \delta_b$ will result in more violation when the front of the comfort zone is violated than when the back is violated, assuming an equal violation area.

Another problem which is directly solved by using the location depending violation is symmetry. Symmetric weighting result in symmetric forces, where through the agents can end up in an equilibrium where there is no movement. Therefore, asymmetry in comfort zones or weighting is desired.

Further research regarding this social force model is implementing different and more accurate agent dynamics. Currently, the unicycle model is adopted to investigate the effect of the constraint. However, this model is not a good representation of a vehicle, a more appropriate model such as the bicycle model should be used. Furthermore, all agents possess the same dynamics and kinematics, i.e. the system is homogeneous, in contrast to real traffic which is typically heterogeneous. Real traffic consists of vehicles with different dynamics and requirements due to their load, engine and dimensions. This could have a great impact on the performance if the agents do not take an appropriate

action, e.g. if there is a slow lorry in front of a passenger car and the speed difference is sufficiently large, it should over take the lorry, if there is space on the adjunct lane.

The ultimate goal is fully autonomous driving with implicit decision making for all scenarios. This is possible with the social force model, where the desired direction term can be replaced with a navigation controller, indicating the required direction of an agent.

Furthermore, the traffic jam problem should also be solved by the autonomous driving systems. In analogy to fluid modeling the speed and density (inter-vehicle distance) before and after a road narrowing should be matched to avoid jams. However, the social force model is only capable of locally implicit decision making and improving the throughput locally. To solve the larger problem, it is interesting to study talking or smart infrastructures, which impose agents their cruise speed and inter-agent distance such that the capacity before and after the road narrowing is matched. The social force model is then used to solve the local merging problems and increases the throughput locally if it is required. The performance of the social force model can be further increased by adding feedforward terms by means of communication, similar to cooperative adaptive cruise control (CACC).

Another important research topic is the emergence of oscillatory flows since the social force model is based on pedestrians, who also create oscillatory flows when queuing [17]. Using a full two-dimensional model and requiring agents to merge, it is hard to define a measure such as string stability. Every merging upper lane agent causes a step response on the string of lower lane agents. This makes it difficult to find a measure of string stability for the complete system.

Bibliography

[1] Rijkswaterstaat, "Publieksrapportage Rijkswegennet 2e periode 2017," report, Ministerie van Infrastructuur en Milieu, Oct. 2017.

[2] ANWB, "Filezwaarte januari & februari 2017." https://www.anwb.nl/verkeer/nieuws/nederland/2017/maart/filezwaarte-januari-februari, Mar. 2017. Accessed: 2017-04-24.

[3] TNO, "Top 15 filelocaties voor verschillende fileoorzaken in Nederland," report, TNO, July 2011.

[4] A. Karimi, A. Hegyi, B. D. Schutter, H. Hellendoorn, and F. Middelham, "Integration of dynamic route guidance and freeway ramp metering using model predictive control," in *Proceedings of the 2004 American Control Conference*, vol. 6, pp. 5533–5538, June 2004.

[5] Spookfiles A58 Ontwikkelingsteam, "Spookfiles A58," tech. rep., Provincie Noord Brabant, July 2014.

[6] J. Zhou and H. Peng, "String stability conditions of adaptive cruise control algorithms," *IFAC Proceedings Volumes*, vol. 37, pp. 649 – 654, Apr. 2004. IFAC Symposium on Advances in Automotive Control 2004, Salerno, Italy, 19-23 April 2004.

[7] J. Ploeg, N. van de Wouw, and H. Nijmeijer, "$\mathcal{L}_p$ string stability of cascaded systems: Application to vehicle platooning," *IEEE Transactions on Control Systems Technology*, vol. 22, pp. 786–793, Mar. 2014.

[8] ACEA, "Truck industry gears up for wide-spread introduction of semi-automated convoys by 2023." Truckindustrygearsupforwide-spreadintroductionofsemi-automatedconvoysby2023, May 2017. Accessed: 2018-08-05.

[9] D. Braess, "Über ein paradoxon aus der verkehrsplanung," *Unternehmensforschung*, vol. 12, pp. 258–268, Dec. 1968.

[10] C. Englund, L. Chen, J. Ploeg, E. Semsar-Kazerooni, A. Voronov, H. H. Bengtsson, and J. Didoff, "The grand cooperative driving challenge 2016: Boosting the introduction of cooperative automated vehicles," *IEEE Wireless Communications*, vol. 23, pp. 146–152, Aug. 2016.

[11] E. Semsar-Kazerooni and J. Ploeg, "Interaction protocols for cooperative merging and lane reduction scenarios," in *2015 IEEE 18th International Conference on Intelligent Transportation Systems*, pp. 1964–1970, Sept. 2015.

[12] E. Semsar-Kazerooni, K. Elferink, J. Ploeg, and H. Nijmeijer, "Multi-objective platoon maneuvering using artificial potential fields," *IFAC-PapersOnLine*, vol. 50, pp. 15006 – 15011, July 2017. 20th IFAC World Congress.

[13] D. Kostić, S. Adinandra, J. Caarls, N. van de Wouw, and H. Nijmeijer, "Collision-free tracking control of unicycle mobile robots," in *Proc. 48h IEEE Conf. Decision and Control (CDC) held jointly with 2009 28th Chinese Control Conf*, pp. 5667–5672, Dec. 2009.

[14] T. Vicsek, A. Czirók, E. B. Jacob, I. Cohen, and O. Shocket, "Novel type of phase transition in a system of self-driven particles," *Physical Review Letters*, vol. 75, pp. 1226–1229, Aug. 1995.

[15] B. Fitzgerald, J. Padding, and R. van Santen, *Collective motion*, ch. Modelling of Collective Motion. Singapore: World Scientific, 2019.

[16] C. K. Hemelrijk and H. Hildenbrandt, "Schools of fish and flocks of birds: their shape and internal structure by self-organization," *Interface Focus*, vol. 2, pp. 726–737, Aug. 2012.

[17] D. Helbing, L. Buzna, A. Johansson, and T. Werner, "Self-organized pedestrian crowd dynamics: Experiments, simulations, and design solutions," *Transportation Science*, vol. 39, pp. 1–24, Feb. 2005.

[18] V. Gazi and K. M. Passino, *Swarm Stability and Optimization*. Springer, 2011.

[19] M. Brambilla, E. Ferrante, M. Birattari, and M. Dorigo, "Swarm robotics: a review from the swarm engineering perspective," *Swarm Intelligence*, vol. 7, pp. 1–41, Mar. 2013.

[20] D. Helbing and P. Molnár, "Social force model for pedestrian dynamics," *Physical Review E*, vol. 51, pp. 4282–4286, May 1995.

[21] D. Helbing, I. Farkas, and T. Vicsek, "Simulating dynamical features of escape panic," *Letters to Nature*, vol. 407, pp. 487–490, Sept. 2000.

[22] A. Rodriguez-Angeles, H. Nijmeijer, and F. J. M. van Kuijk, *A Bio-inspired Autonomous Navigation Controller for Differential Mobile Robots Based on Crowd Dynamics*, pp. 553–560. Cham: Springer International Publishing, June 2016.

[23] H. Hildenbrandt, C. Carere, and C. K. Hemelrijk, "Self-organized aerial displays of thousands of starlings: a model," *Behavioral Ecology*, vol. 21, pp. 1349–1359, Oct. 2010.

[24] S. S. Ge and Y. J. Cui, "Dynamic motion planning for mobile robots using potential field method," *Autonomous robots*, vol. 13, pp. 207–222, Nov. 2002.

[25] H. G. Tanner, A. Jadbabaie, and G. J. Pappas, *Flocking in Teams of Nonholonomic Agents*, pp. 229–239. Berlin, Heidelberg: Springer Berlin Heidelberg, 2005.

[26] W. M. Spears, D. F. Spears, J. C. Hamann, and R. Heil, "Distributed, physics-based control of swarms of vehicles," *Autonomous Robots*, vol. 17, pp. 137–162, Sept. 2004.

[27] E. Ferrante, A. E. Turgut, C. Huepe, A. Stranieri, C. Pinciroli, and M. Dorigo, "Self-organized flocking with a mobile robot swarm: a novel motion control method," *Adaptive Behavior*, vol. 20, pp. 460–477, Dec. 2012.

[28] H. Pei, S. Chen, and Q. Lai, "A local flocking algorithm of multi-agent dynamic systems," *International Journal of Control*, vol. 88, pp. 2242–2249, Apr. 2015.

[29] E. Şahin, *Swarm Robotics: From Sources of Inspiration to Domains of Application*, pp. 10–20. Berlin, Heidelberg: Springer Berlin Heidelberg, 2005.

[30] M. W. Spong, S. Hutchinson, and M. Vidyasagar., *Robot Modeling and Control*, vol. 3. John Wiley & Sons, Inc., 2006.

[31] M. T. Wolf and J. W. Burdick, "Artificial potential functions for highway driving with collision avoidance," in *2008 IEEE International Conference on Robotics and Automation*, (Pasadena, CA, USA), pp. 3731–3736, May 2008.

[32] D. Reichardt and J. Shick, "Collision avoidance in dynamic environments applied to autonomous vehicle guidance on the motorway," in *Intelligent Vehicles' 94 Symposium, Proceedings of the*, pp. 74–78, IEEE, Nov. 1994.

[33] J. C. Gerdes and E. J. Rossetter, "A unified approach to driver assistance systems based on artificial potential fields," *Journal of Dynamic Systems, Measurement, and Control*, vol. 123, pp. 431–438, Sept. 2001.

[34] B. Schiller, V. Morellas, and M. Donath, "Collision avoidance for highway vehicles using the virtual bumper controller," in *Proceedings of the IEEE International Symposium on Intelligent Vehicles*, pp. 28–30, Dec. 1998.

[35] E. J. Rossetter, J. P. Switkes, and J. C. Gerdes, "Experimental validation of the potential field lanekeeping system," *International journal of automotive technology*, vol. 5, pp. 95–108, Jan. 2004.

[36] E. Semsar-Kazerooni, J. Verhaegh, J. Ploeg, and M. Alirezaei, "Cooperative adaptive cruise control: An artifical potential field approach," in *IEEE Intelligent Vehicles Symposium (IV)*, (Gothenburg, Sweden), June 2016.

[37] École Polytechnique Fédérale de Lausanne, "e-puck." http://www.e-puck.org/, 2017. Accessed: 2017-01-20.

[38] A. De Luca, G. Oriolo, and M. Vendittelli, "Stabilization of the unicycle via dynamic feedback linearization," *IFAC Proceedings Volumes*, vol. 33, no. 27, pp. 687–692, 2000.

[39] M. J. Lighthill and G. Whitham, "On kinematic waves II. A theory of traffic flow on long crowded roads," *Proceedings of the Royal Society of London A: Mathematical, Physical and Engineering Sciences*, vol. 229, pp. 317–345, May 1955.

[40] C. P. L. Veeger, L. F. P. Etman, J. van Herk, and J. E. Rooda, "Generating cycle time-throughput curves using effective process time based aggregate modeling," in *2008 IEEE/SEMI Advanced Semiconductor Manufacturing Conference*, pp. 127–133, May 2008.

[41] I. J. B. F. Adan, A. T. Hofkamp, J. Rooda, and J. Vervoort, *Analysis of Manufacturing Systems*, Oct. 2012.

[42] E. Lefeber, *Modeling and Control of Manufacturing Systems*, pp. 9–30. London: Springer London, Mar. 2012.

[43] J. H. Jacobs, L. F. P. Etman, E. J. J. van Campen, and J. E. Rooda, "Characterization of operational time variability using effective process times," *IEEE Transactions on Semiconductor Manufacturing*, vol. 16, pp. 511–520, Aug. 2003.

[44] R. Berg, van den, E. Campen, van, A. Lefeber, L. Etman, and J. Rooda, "Evaluating cycle time performance of integrated metrology," in *Proceedings of the 4th European AEC/APC Conference, 27-28 March 2003, Grenoble, France*, Feb. 2003.

[45] D. Helbing, "Traffic and related self-driven many-particle systems," *Reviews of Modern Physics*, vol. 73, pp. 1067–1141, Oct. 2001.

[46] W. D. Callister, *Materials science and engineering*. New York, NY: Wiley, seventh ed., 2007.

[47] J. ao P. Hespanha, *Linear Systems Theory*. Princeton, N.J. [u.a.]: Princeton University Press, 2009.

[48] H. K. Khalil, *Nonlinear Systems: Pearson New International Edition*. Pearson Education International, 2000.

[49] H. Brezis, *Functional analysis, Sobolev spaces and partial differential equations*. Springer Science & Business Media, 2010.

[50] D. Yanakiev and I. Kanellakopoulos, "Variable time headway for string stability of automated heavy-duty vehicles," in *Decision and Control, 1995., Proceedings of the 34th IEEE Conference on*, vol. 4, pp. 4077–4081, IEEE, Dec. 1995.

[51] D. Yanakiev, J. Eyre, and I. Kanellakopoulos, "Analysis, design, and evaluation of avcs for heavy-duty vehicles with actuator delays," tech. rep., University of California, Apr. 1998.

[52] K. Santhanakrishnan and R. Rajamani, "On spacing policies for highway vehicle automation," *IEEE Transactions on Intelligent Transportation Systems*, vol. 4, pp. 198–204, Dec. 2003.

[53] M. Nieuwenhuijze, "String stability analysis of bidirectional adaptive cruise control," Master's thesis, Eindhoven University of Technology, Dec. 2010.

[54] Autobytel, "What is Adaptive Cruise Control?." https://www.autobytel.com/car-ownership/technology/what-is-adaptive-cruise-control-132514/. Accessed: 2018-06-08.

[55] DAF, "DAF Adaptive Cruise Control." http://www.daf.nl/nl-nl/trucks/comfort-and-safety-systems-euro-6/adaptive-cruise-control, 2015. Accessed: 2018-06-08.

[56] The MathWorks, Inc., "Adaptive Cruise Control system using Model Predictive Control." https://nl.mathworks.com/help/mpc/examples/design-an-adaptive-cruise-control-system-using-model-predictive-control.html, 2016. Accessed: 2018-06-08.

[57] L. W. Tu, *An Introduction to Manifolds*, ch. 13 Bump Functions and Partitions of Unity, pp. 140–148. Universitext, Springer, second ed., June 2010.

Appendix A

Definition of a smooth bump function

The goal of this appendix is to derive a $\mathcal{C}^\infty$ bump function. Within this report, the definition of a bump function by Tu [57] is adopted.

Let q be a point in manifold M, and U a neighborhood of q. By a *bump function at q supported in U* we mean any continuous nonnegative function ψ on M that is 1 in a neighborhood of q with $\text{supp}(\psi) \subset U$. The support of a real-valued function f on a manifold M is defined to be the closure in M of the subset on which $f \neq 0$:

$$\text{supp}(f) = \text{closure of } \{q \in M | f(q) \neq 0\} \text{ in } M.$$

In Figure A.1 a bump function at q is shown. Let a, b, c, d be arbitrary constants where $a < b \leq c < d$. The bump function ψ is nonzero on the open interval (a, d), its support is the closed interval $[a, d]$. Furthermore the function is 1 in the closed interval $[b, c]$. Summarizing

$$\psi(z) = \begin{cases} 0 & \text{for} \quad z \leq a \\ 1 & \text{for } b \leq z \leq c \\ 0 & \text{for} \quad z \geq d \end{cases}$$

for $z \in \mathbb{R}$.

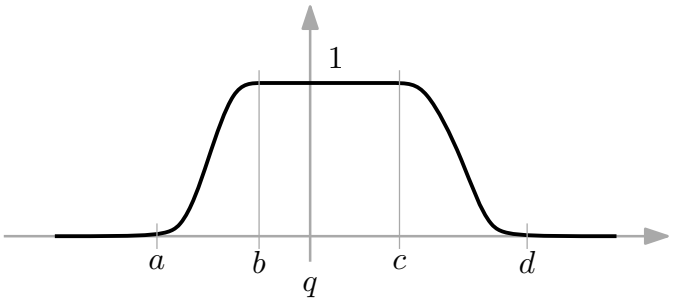

Figure A.1: A bump function at q on $\mathbb{R}$.

Based on the work of Tu [57], a bump function can be constructed from a smooth version of the step function. Consider the $\mathcal{C}^\infty$ function

$$f(t) := \begin{cases} e^{-1/t} & \text{for } t > 0 \\ 0 & \text{for } t \leq 0 \end{cases}. \tag{A.1}$$

A smooth step function $g(t)$ is then obtained via

$$g(t) := \frac{f(t)}{f(t) + f(1-t)}. \tag{A.2}$$

The denominator of $g(t)$ is never zero since for $t > 0$, $f(t) > 0$ and therefore $f(t) + f(1-t) \geq f(t) > 0$. For $t \leq 0$ holds that $1 - t \geq 1$ and therefore $f(t) + f(1-t) \geq f(1-t) > 0$. Thus in both cases $f(t) + f(1-t) \neq 0$, hence $g(t)$ is defined for all t.

For $t \geq 1$, $f(1-t) = 0$, therefore the function $g(t) = f(t)/f(t)$ is identically 1. For $t \leq 0$, the numerator $f(t)$ is 0 and so is $g(t)$, since the denominator is never zero. Hence the function $g(t)$ is a smooth step function with the desired properties (see Figure A.2).

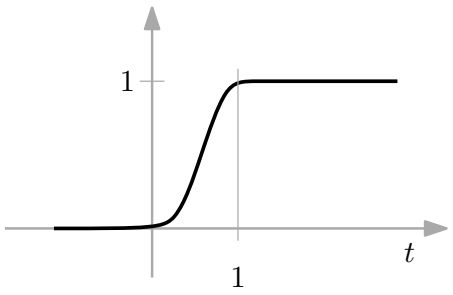

Figure A.2: Smooth step function $g(t)$.

Within the work of Tu [57] the bump function at q is symmetric over the axis q. To create a non-symmetric bump function, we deviate from Tu its work.

The bump function can be constructed from two smooth step functions. One step function describing the left of the bump, the ramp up, $\psi^+(z)$. The other function describing the right part of te bump, the ramp down, $\psi^-(z)$.

To create the smooth step function $\psi^+(z)$ such that

$$\psi^+(z) = \begin{cases} 0 & \text{for } z \leq a \\ 1 & \text{for } z \geq b \end{cases}$$

a linear change of variables is made to map $[a, b]$ to $[0, 1]$

$$z \mapsto \frac{z-a}{b-a}$$

where $a < b$. By setting this mapping as argument of $g(t)$, the desired smooth step function is obtained

$$\psi^+(z) := g\left(\frac{z-a}{b-a}\right). \tag{A.3}$$

The same method is applied for the function describing the ramp down $\psi^-(z)$, where $[c, d]$ is mapped to $[-1, 0]$

$$z \mapsto \frac{z-d}{c-d}$$

with $c < d$. Setting the mapping as argument of the smooth step function $g(t)$

$$\psi^-(z) := g\left(\frac{z-d}{c-d}\right). \tag{A.4}$$

The total smooth bump function is created by multiplying both smooth step functions

$$\psi(z) := \psi^+(z)\psi^-(z) = g\left(\frac{z-a}{b-a}\right) g\left(\frac{z-d}{c-d}\right). \tag{A.5}$$

Here $\psi(z)$ is a C^∞ bump function in $\mathbb{R}$ that is identically 1 on $[b, c]$ and 0 on $(-\infty, a]$ and $[d, \infty)$. To get a C^∞ bump function $\Psi : \mathbb{R}^n \to \mathbb{R}$ the product of the bump functions are taken

$$\Psi(\mathbf{z}) := \prod_{i=1}^{n} \psi(z_i), \tag{A.6}$$

with $\mathbf{z} := \begin{pmatrix} z_1 & \dots & z_n \end{pmatrix}$.

Appendix B

Rewriting the constraint to obtain kinematic inputs

The social force model (2.2) generates a generalized force for agent i. Via Newton's second law, this can be transformed to the desired acceleration $\mathbf{a}_i^d$. However the desired acceleration cannot be directly used as an input for the unicycle kinematics due to the nonholonomic constraint. The inputs of the unicycle model are the forward velocity v_i and rotation speed ω_i.

Within the work of Rodriguez-Angeles et al. [22] the nonholonomic constraint is rewritten to obtain the desired inputs. First, the desired velocity is defined as $\mathbf{a}_i^d =: \dot{\mathbf{v}}_i^d$. The speed of an unicycle is than set to the magnitude of the desired velocity

$$v_i := ||\mathbf{v}_i^d|| = \sqrt{\left(v_{i,x}^d\right)^2 + \left(v_{i,y}^d\right)^2}. \tag{B.1}$$

The nonholonomic constraint of the unicycle

$$\ddot{y}_i \dot{x}_i - \ddot{x}_i \dot{y}_i = v_i^2 \omega_i \tag{B.2}$$

can be rewritten to the required rotational velocity

$$\omega_i = \frac{\ddot{y}_i \dot{x}_i - \ddot{x}_i \dot{y}_i}{v_i^2}. \tag{B.3}$$

With the assumption that the desired velocity is equal to the real unicycle velocity: $\ddot{x}_i = a_{i,x}^d$; $\ddot{y}_i = a_{i,y}^d$; $\dot{x}_i = v_{i,x}^d$; and $\dot{y}_i = v_{i,y}^d$, the following control strategy is obtained

$$\omega_i := \frac{a_{i,y}^d v_{i,x}^d - a_{i,x}^d v_{i,y}^d}{\epsilon + ||\mathbf{v}_i^d||^2}, \tag{B.4}$$

where $0 < \epsilon \ll 1$ to avoid singularities when $v_i = 0$.

The problem with this method is that the orientation is not taken into account when setting the forward speed. The forward speed of the unicycle is directly set to the magnitude of the desired velocity, while it does not have the desired orientation. The orientation is of the unicycle is changed by adjusting the rotation speed via the expression in (B.4). Therefore the agent will initially move into the wrong direction increasing the error.

Applying this method in combination with the social force model, will result in instability. The agent will drive into the wrong direction, therefore the social force model will increase the desired control action (i.e. increasing the desired velocity), causing a larger error.

The problem is visualized in Figure B.1 by using snapshots from the simulation. Within the shown scenario there are only two agents present, which already causes the unstable behavior.

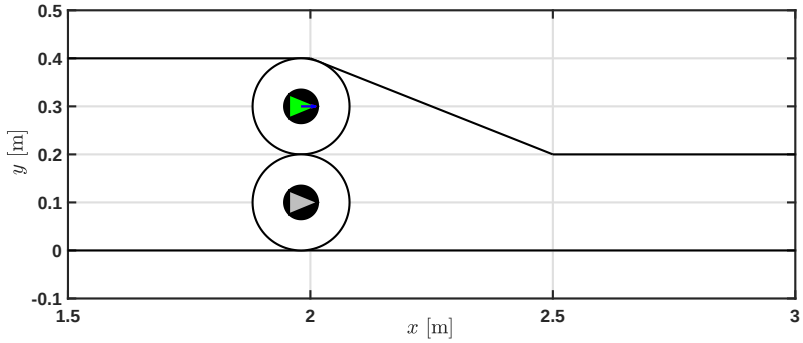

(a) t_0

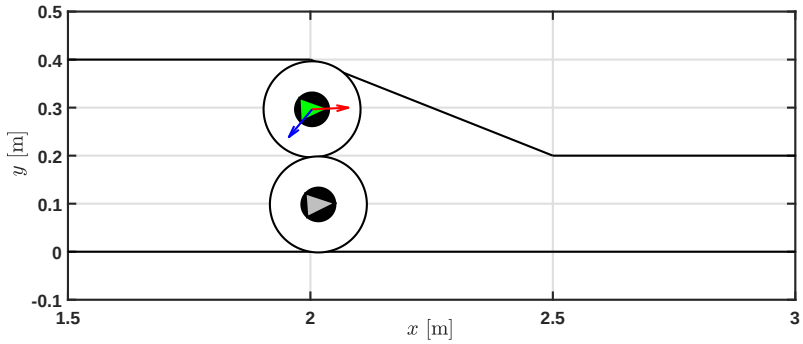

(b) t_1

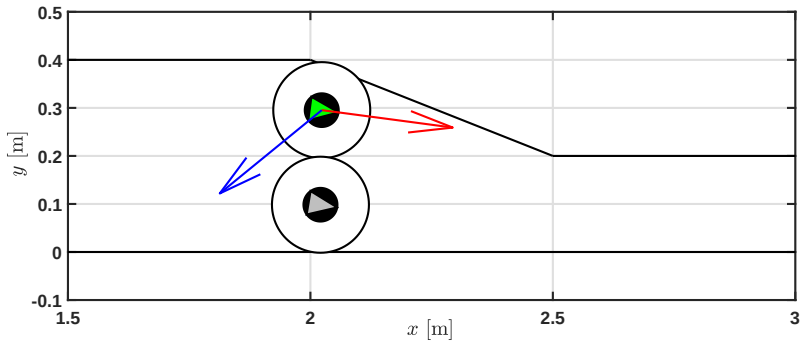

(c) t_2

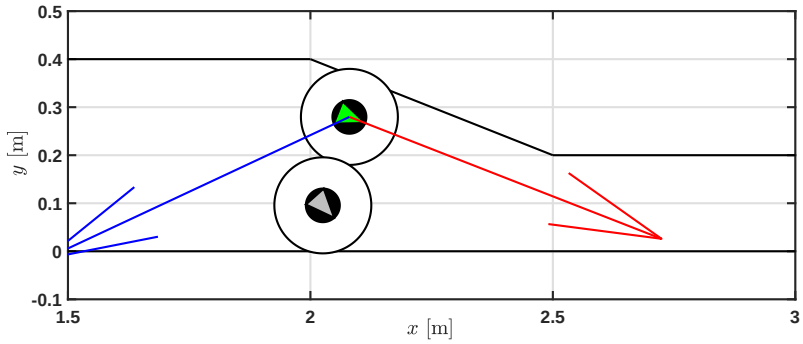

(d) t_3

Figure B.1: Four snapshots from a simulation with the rewritten constraint strategy of Rodriguez-Angels et al.. The red arrow represents the agent velocity while the blue arrow represents the desired velocity. By setting the forward velocity equal to the magnitude of the desired velocity without taking the orientation into account, the agent drives in the wrong direction increasing the desired control action created by the social force model.

Appendix C

Spacing policy 1D case analysis

To gain insight in the effect of the spacing policy on the agent behavior the 2D scenario is simplified to a 1D case. The unicycle kinematics (and control) are neglected, thus a point mass is considered within this case. This results in the following simplified model

$$\begin{aligned} \dot{x}_i &:= v_i \\ \dot{v}_i &:= \frac{1}{m_i}\left(m_i \frac{v_i^c - v_i}{\tau_i} + k_i \operatorname{sign}(x_i - x_j) \max(r_{ij} - d_{ij}, 0)\right) \end{aligned} \tag{C.1}$$

with $r_{ij} := r_i + r_j$ and $d_{ij} := ||x_i - x_j||$. For further simplification, it is assumed that agent j stands still on the origin and cannot move, i.e. $x_j = 0$ and $v_j = 0$. The desired speed is chosen to be zero $v_i^c = 0$, while all other parameters are chosen to be 1, except h_i, r_i, r_j. This results in

$$\begin{aligned} \dot{x}_i &= v_i \\ \dot{v}_i &= -v_i + \operatorname{sign}(x_i) \max(r_{ij} - |x_i|, 0)\,. \end{aligned} \tag{C.2}$$

With the linear spacing policy $r_i := r_{i,0} + h_i|v_i|$ the system can rewritten as

$$\begin{aligned} \dot{x}_i &= v_i \\ \dot{v}_i &= -v_i + \operatorname{sign}(x_i) \max(r + h_i|v_i| - |x_i|, 0)\,, \end{aligned} \tag{C.3}$$

where $r := r_{i,0} + r_{j,0}$. This system can be seen as a piecewise linear system. The phase portraits of this system for different headway-times h_i are drawn in Figures C.1a to C.1c, where the switching lines are indicate by the red dashed lines. It can be seen that for relatively low headway-times the speed will converge to the desired cruise speed. However for large headway-times the system will not converge, since the speed keeps increasing more than the amount of violation is reduced. Therefore the system will not reach the switching line, where the comfort zone stops growing and converge to the desired speed.

This problem could be solved by applying a limit on the comfort zone size, however a more "natural" way is desired. Therefore the problem is solved by changing the gradient of the potential field with a quadratic speed regulation term

$$\left(1 + \gamma_i \frac{||v_i^c \mathbf{e}^d - \mathbf{v}_i||}{\tau_i}\right) \frac{v_i^c \mathbf{e}^d - \mathbf{v}_i}{\tau_i} \tag{C.4}$$

which will be

$$(1 + |v_i|)\, v_i \tag{C.5}$$

in the 1D scenario. Hence the complete model is

$$\begin{aligned} \dot{x}_i &:= v_i \\ \dot{v}_i &:= -(1 + |v_i|)v_i + \operatorname{sign}(x_i) \max(r_{i,0} + r_{j,0} + h_i|v_i| - |x_i|, 0)\,. \end{aligned} \tag{C.6}$$

The phase portraits of this system for different h_i are drawn in Figures C.1d to C.1f. It can be seen that the quadratic term is the winning term for higher speeds, since the zero isocline is not linear anymore but encloses the repulsive field. Therefore the trajectory will always converge to the desired speed.

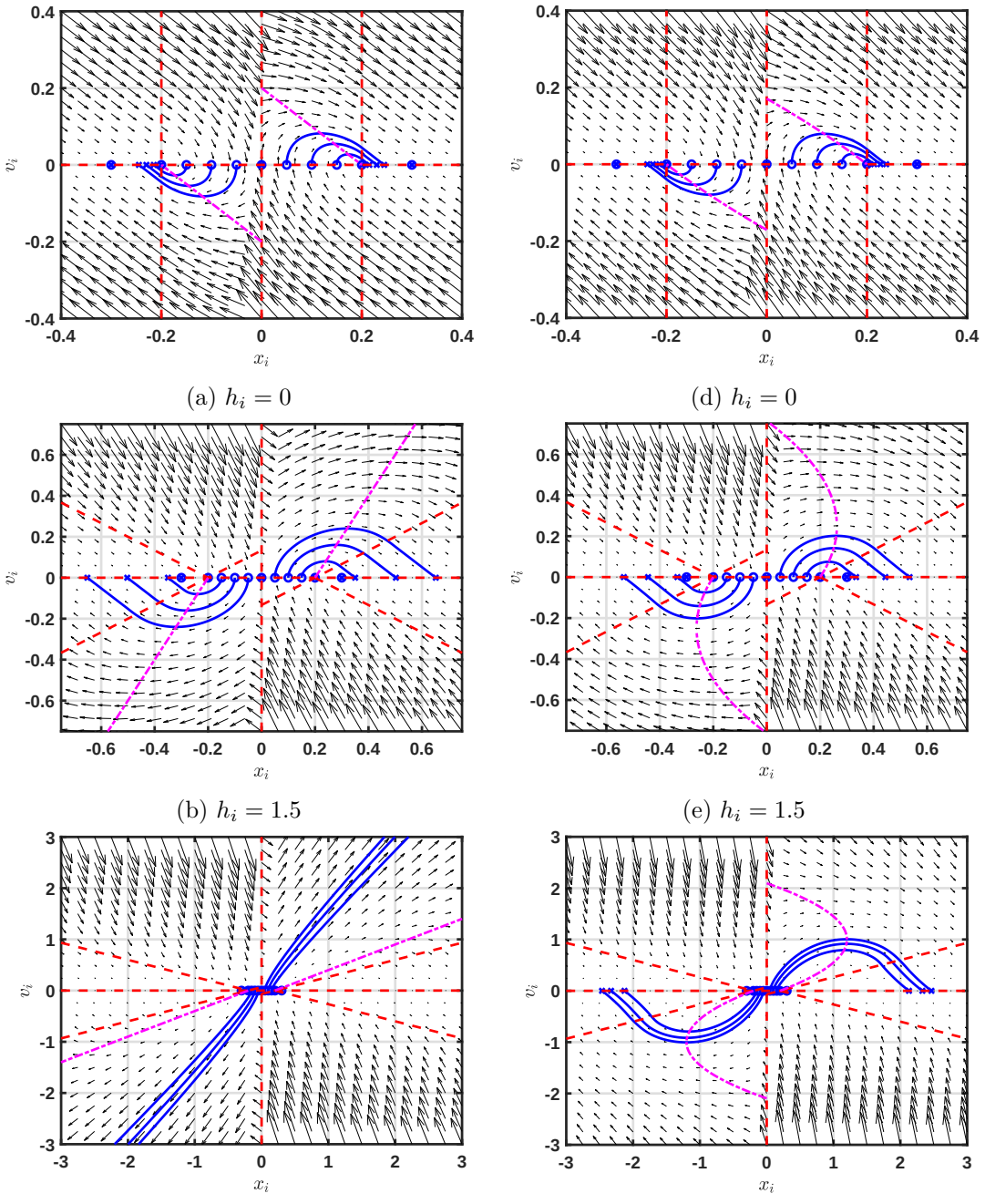

(a) $h_i = 0$ (d) $h_i = 0$

(b) $h_i = 1.5$ (e) $h_i = 1.5$

(c) $h_i = 3$ (f) $h_i = 3$

Figure C.1: Phase portrait of the linear spacing policy with the original linear speed regulation (a, b, c) and the quadratic speed regulation (d, e, f) for different headway-times h_i. The red dashed lines are the switching lines of the piecewise linear system. The blue lines represent the trajectories from the initial condition (circle) to an equilibrium point (cross). The magenta lines indicate the zero isoclines.